BLIND CHANNEL ESTIMATION IN OFDM SYSTEMS

A THESIS SUBMITTED TO
THE GRADUATE SCHOOL OF NATURAL AND APPLIED SCIENCES
OF
MIDDLE EAST TECHNICAL UNIVERSITY

BY

MEHMET AKIF AYAS

IN PARTIAL FULFILLMENT OF THE REQUIREMENTS
FOR
THE DEGREE OF MASTER OF SCIENCE
IN
ELECTRICAL AND ELECTRONICS ENGINEERING

APRIL 2015

Approval of the thesis:

BLIND CHANNEL ESTIMATION IN OFDM SYSTEMS

submitted by **MEHMET AKIF AYAS** in partial fulfillment of the requirements for the degree of **Master of Science in Electrical and Electronics Engineering Department, Middle East Technical University** by,

Prof. Dr. Gülbin Dural Ünver _____
Dean, Graduate School of **Natural and Applied Sciences**

Prof. Dr. Gönül Turhan Sayan _____
Head of Department, **Electrical and Electronics Engineering**

Assoc. Prof. Dr. Melek Diker Yücel _____
Supervisor, **Electrical and Electronics Eng. Dept., METU**

Examining Committee Members:

Prof. Dr. Yalçın Tanık
Electrical and Electronics Engineering Dept., METU _____

Assoc. Prof. Dr. Melek Diker Yücel
Electrical and Electronics Engineering Dept., METU _____

Prof. Dr. Ali Özgür Yılmaz
Electrical and Electronics Engineering Dept., METU _____

Assoc. Prof. Dr. Çağatay Candan
Electrical and Electronics Engineering Dept., METU _____

Assoc. Prof. Dr. Emre Aktaş
Electrical and Electronics Engineering Dept., Hacettepe University _____

Date: _____

I hereby declare that all information in this document has been obtained and presented in accordance with academic rules and ethical conduct. I also declare that, as required by these rules and conduct, I have fully cited and referenced all material and results that are not original to this work.

Name, Last Name: MEHMET AKIF AYAS

Signature :

ABSTRACT

BLIND CHANNEL ESTIMATION IN OFDM SYSTEMS

Ayas, Mehmet Akif
M.S., Department of Electrical and Electronics Engineering
Supervisor : Assoc. Prof. Dr. Melek Diker Yücel

April 2015, 75 pages

In this thesis, we have studied blind channel estimation methods for single-input-multiple-output (SIMO) orthogonal frequency division multiplexing (OFDM) systems in time and frequency domain, in which the cross relation between the channel gains and a single snapshot of the received signal on each subcarrier is utilized.

We have performed blind channel estimation for uncorrelated and correlated Rayleigh fading channel pairs using time and frequency methods in OFDM systems with one-transmitting, two-receiving antennas. Using time and frequency methods, blind channel estimation simulations have been run for different channel lengths, different number of subcarriers and different modulation schemes; i.e., QPSK and 16-QAM. Channel estimation results have been used to calculate the normalized root mean squared errors. Besides, using Zero Forcing (ZF) and Minimum Mean Squared Error (MMSE) equalizers with Maximum Likelihood (ML) estimators in receiver side, we have estimated symbols that are used for transmission and bit error probabilities have been calculated with the estimated symbols.

These simulations have been repeated with one-transmitting, three-receiving and one-transmitting, four-receiving antennas in order to observe the effect of antenna diversity over the SIMO-OFDM systems.

Keywords: SIMO Systems, OFDM, Cross Relation, Blind Channel Estimation

ÖZ

DİKEY FREKANS BÖLMELİ ÇOKLAMA SİSTEMLERİNDE KÖR KANAL KESTİRİMİ

Ayas, Mehmet Akif
Yüksek Lisans, Elektrik ve Elektronik Mühendisliği Bölümü
Tez Yöneticisi : Doç. Dr. Melek Diker Yücel

Nisan 2015 , 75 sayfa

Bu tezde, kanal kazançları ile birim zamanda alınan her taşıyıcıdaki sinyal ilişkisinin kullanıldığı, tek-girişli-çok-çıkışlı dikey frekans bölmeli çoklama (OFDM) sistemleri için zaman bölgesi ve frekans bölgesinde kör kanal kestirim yöntemleri üzerinde çalışıldı.

Dikey frekans bölmeli çoklama modülasyonunun kullanıldığı bir-gönderici, iki-alıcı antenli sistemde, Rayleigh sönümlü ilişkili ve ilişkisiz kanal çiftleri kullanılarak zaman ve frekans yöntemleriyle kör kanal kestirimi yapıldı. Zaman ve frekans yöntemleriyle kör kanal kestirimi işlemleri, farklı uzunluklardaki kanal çiftleri, farklı sayıdaki alt taşıyıcılar ve QPSK ile 16-QAM modülasyon türleri için tekrarlandı. Kanal kestirimi çıktıları kullanılarak normalize-karekök-ortalama-hatası hesaplamaları yapıldı. Ayrıca, almaçlarda, sıfıra-zorlayan (ZF) ve en küçük-kare-ortalama-hatası (MMSE) denkleştiricileri, en büyük-benzerlik (ML) kestiricisi ile kullanılarak iletişimde kullanılan sembollerin kestirimi yapıldı ve ikil (bit) hata olasılıkları kestirilen semboller yardımıyla hesaplandı.

Anten çeşitliliğinin SIMO-OFDM sistemler üzerindeki etkisini gözlemlemek için bu simülasyonlar bir-gönderici, üç-alıcı antenli sistemler ve bir-gönderici, dört-alıcı antenli sistemler için tekrarlandı.

Anahtar Kelimeler: Tek Giriş Çok Çıkışlı Sistemler, Dikey Frekans Bölmeli Çoklama, Çapraz İlişki, Kör Kanal Kestirimi

To my family

ACKNOWLEDGMENTS

I would like to thank my supervisor Melek Diker Yücel for being there for me whenever I needed her help and guidance, regardless of time and date. It was a great honor and pleasure to work with her during my thesis work. Her knowledge, patience and understanding affected me in remarkable ways that will surely help me in my future academic and professional life.

I would also like to express my gratitude to my colleague Şeniz Şener Usanmaz and my bosses Kıvanç Baş and Ömür Baş at Promod Research and Software for their advice and guidance throughout my Master's education.

Many sincere thanks to Janan Mali for her friendship and encouragement. Also special thanks to Bahar Yılmaz, İbrahim Nergiz, Ahmet Emre Topbaş and Kaan Ergün for the motivation and emotional support they provided.

Last but not the least, sincerest thanks to my parents Nedim and Atni, my older sisters Hatice and Meryem, and my brother-in-law Cenk Erdoğan for supporting and believing in me all my life.

TABLE OF CONTENTS

LIST OF TABLES

TABLES

LIST OF FIGURES

FIGURES

LIST OF ABBREVIATIONS

ARE	Antenna Relation Estimation
AWGN	Additive White Gaussian Noise
BER	Bit Error Ratio
CIR	Channel Impulse Response
CRB	Cramer Rao Bound
CP	Cyclic Prefix
DFT	Discrete Fourier Transform
FIM	Fisher Information Matrix
ICI	Inter Carrier Interference
IDFT	Inverse Discrete Fourier Transform
ISI	Inter Symbol Interference
LOS	Line of Sight
MIMO	Multiple Input Multiple Output
MAE	Mean Absolute Error
MSE	Mean Squared Error
MMSE	Minimum Mean Squared Error
NRMSE	Normalized Root Mean Squared Error
OFDM	Orthogonal Frequency Division Multiplexing
PSK	Phase Shift Keying
QAM	Quadrature Amplitude Modulation
SIMO	Single Input Multiple Output
SRE	Subcarrier Relation Estimation
ZF	Zero Forcing

CHAPTER 1

INTRODUCTION

1.1 Orthogonal Frequency Division Multiplexing

Orthogonal Frequency Division Multiplexing (OFDM) is a frequency division multiplexing scheme used for encoding digital data on multiple carrier frequencies. OFDM has developed into a popular scheme for wideband digital communication, whether wireless or over copper wires, and it is used in applications such as digital television and audio broadcasting, DSL Internet access, wireless networks, powerline networks, and 4G mobile communications [1]. Bandwidth is divided into a large number of closely spaced subcarriers and these subcarriers are used to carry data over parallel data streams. Each subcarrier is modulated with a modulation method such as Phase Shift Keying (PSK) or Quadrature Amplitude Modulation (QAM) at a low symbol rate.

1.2 Mathematical Representation of OFDM

OFDM is a frequency division multiplexing system, in which subcarriers are orthogonal to each other. FDM System is illustrated in Figure 1.1. For one-symbol duration, frequency-multiplexed digitally modulated signal can be written as,

$$x(t) = \sum_{n=0}^{N-1} s_{n,l} e^{j2\pi f_n t} \text{ for } lT \leq t \leq (l+1)T \tag{1.1}$$

where an OFDM block with of N information symbols $s_{n,l}$ is transmitted synchronously, l is the block count, f_n is the frequency of the n^{th} subcarrier and

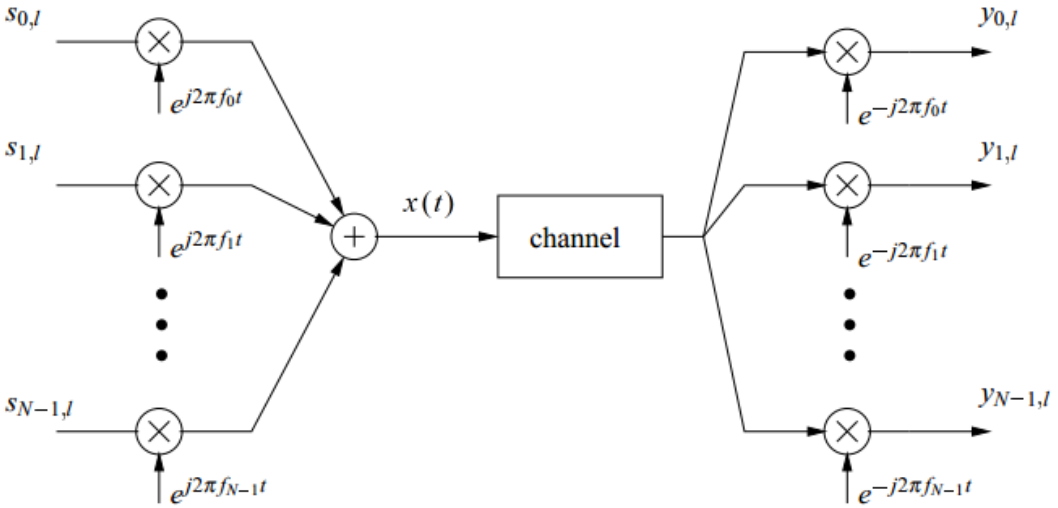

Figure 1.1: FDM system

T is the symbol duration. In OFDM system, the orthogonality condition is satisfied as,

$$\int_0^T e^{j2\pi f_a t} e^{-j2\pi f_b t}\, dt = \int_0^T e^{j2\pi (f_a - f_b) t}\, dt = 0 \tag{1.2}$$

meaning the space between subcarrier frequencies should be

$$\Delta f = f_a - f_b = \frac{m}{T} \tag{1.3}$$

where m is any integer. In order to preserve the orthogonality, the smallest frequency separation between adjacent subcarriers should be at least $1/T$.

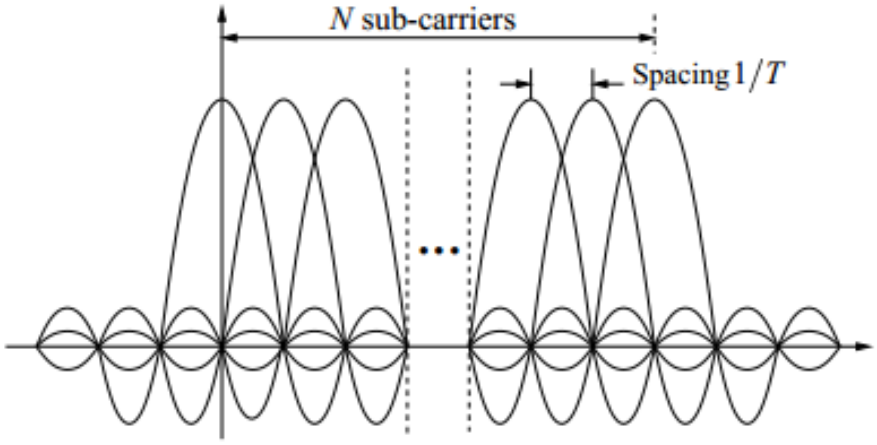

Figure 1.2: OFDM system with N subcarriers

Using orthogonality, each subcarrier can be demodulated at the receiver without suf-

fering from Intercarrier Interference (ICI). As shown in Figure 1.2 passbands of the subcarriers may overlap in OFDM systems. This allows one to use frequency band in a most efficient manner as shown in Figure 1.3.

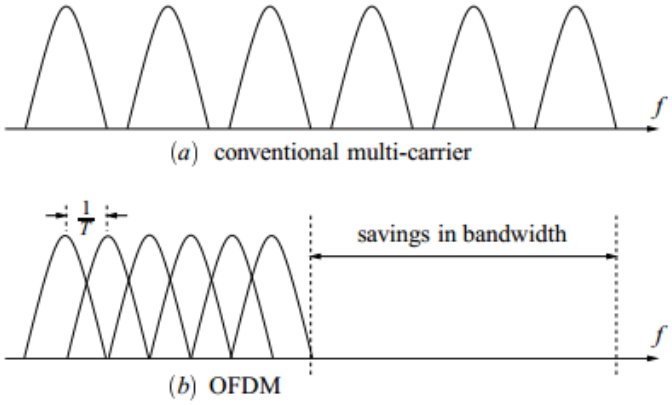

Figure 1.3: Comparison between the conventional multi-carrier technique and OFDM

OFDM signal $x(t)$ can be represented as a combination of digital signals as following equation by substituting $t = \frac{kT}{N}$ and $f_n = \frac{n}{T}$

$$x(t) \mid_{t=k\frac{T}{N}} = \sum_{n=0}^{N-1} s_{n,l} e^{j2\pi \frac{n}{T} k \frac{T}{N}} = \sum_{n=0}^{N-1} s_{n,l} e^{j2\pi \frac{nk}{N}} \quad \text{for} \quad k = 0, 1, ..., N-1 \qquad (1.4)$$

Then, the implementation of OFDM scheme becomes very efficient using the Fast Fourier Transform (FFT) algorithm. Discrete Fourier Transform (DFT) implementation of the transmitted signal is shown in Figure 1.4.

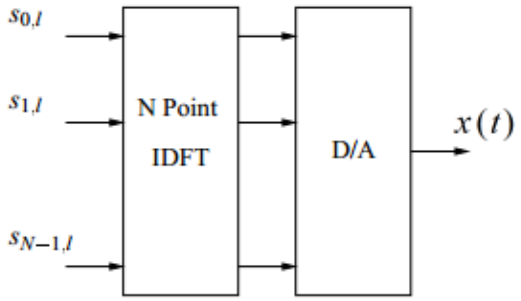

Figure 1.4: DFT implementation of transmitted signal

1.3 History of OFDM

In the 60s, Robert W. Chang presented his paper about basic principles of OFDM [2]. The difference of the developed system from the traditional systems is that the mutually orthogonal subcarriers overlap in the spectrum. Orthogonality principle of OFDM makes the use of steep bandpass filters unnecessary, which were used in old multi-carrier modulation systems to distinguish the spectra of the subcarriers. In 1967, Saltzberg [3] worked on the performance of the OFDM and concluded that "the strategy of designing an efficient parallel system should concentrate more on reducing crosstalk between adjacent channels than on perfecting the individual channels themselves, since the distortions due to crosstalk tend to dominate."

In 1971, Ebert and Weinstein [4] proposed to apply DFT and IDFT to achieve baseband modulation and demodulation in OFDM systems. Their study contributed to eliminating the bank of subcarrier oscillators and leading efficient processing. Current OFDM systems apply FFT and IFFT to perform modulation and demodulation of the information data and their study made OFDM technology more practical.

In 1980, Peled and Ruiz [5] presented the concept of cyclic prefix in order to remove the intercarrier interference (ICI). In cyclic prefix method, cyclic extension of OFDM symbols (last C_p symbols) are appended to the time domain signal instead of using empty guard spaces in time between OFDM symbols.

OFDM technology has been used in many applications. Application areas of OFDM are shown in Table 1.1.

Table 1.1: Application areas of OFDM

Broadcasting	Digital Audio Broadcasting
	Digital Video Broadcasting
	High definition television terrestrial broadcasting
DSL Networks	Asymmetric Digital Subscriber Line
	High bit rate Digital Subscriber Line
	Very high speed Digital Subscriber Line
WLAN	IEEE 802.11 a/g/n/ac
	HiperLAN2
Others	WiMax
	4G mobile communication networks
	High Rate Wireless PAN (802.15.3.a)

1.4 Previous Work on Channel Estimation for OFDM

OFDM is widely used in wireless communication systems to support high data rates. In OFDM Systems, dividing bandwidth into a large number of closely spaced subcarriers a high data rate is achieved. Since the channel information is needed for coherent detection, various channel estimation techniques are developed for OFDM systems. These techniques can be classified in two main groups; training symbol based algorithms and blind channel estimation techniques.

In training symbol based algorithms, training sequence pilots are added in time or frequency domain that enables estimation of the channels at the pilot positions [6–8]. Pilot schemes enable high estimation performance at the expense of bandwidth efficiency because of additional resources [9, 10]. These schemes add some complexity in the system, since both the transmitter and the receiver must have a built-in a priori knowledge about the pilot scheme and both must perform extra processing to implement the pilot scheme [11]. However, in blind channel estimation techniques there is no need to transmit training symbols.

Compared to schemes using training sequences, blind channel estimation methods for SIMO-OFDM systems are claimed to have the advantage of saving bandwidth, improving energy efficiency and system throughput by using only the channel outputs [12]. On the other hand, they have the disadvantages of high BER results [13], requirement of accurate channel length estimation and large amount of computation for the singular value decomposition [14]. Based on the information used for esti-

mation, blind channel estimation techniques can be categorized in two groups; the statistical subspace methods and deterministic methods. Statistical subspace methods [9, 10] require steady channel conditions for a long period of time and a large number of data in order to obtain statistical information about the channel, thus these methods are not suitable for high speed wireless communications. On the other hand, in deterministic methods, only the received data is used for estimation and these methods are appropriate for fast channel estimation problems.

In [15, 16] blind methods for SIMO-OFDM systems without cyclic prefix (CP) have been proposed. In [12] a study has been performed for zero padding based SIMO-OFDM systems using a single OFDM block and computational complexity, memory usage and estimation performance of this method has been compared with cyclic prefix based SIMO-OFDM blind channel estimation method in [17].

The deterministic method with CP-based SIMO-OFDM with one-transmitting and two-receiving antennas has been proposed in [18, 19]. In these studies, multipath channel gains are estimated in time domain using cross relations between antennas with a single OFDM block. However, number of the unknown estimation parameters increases as the channel length is increased. Moreover in [17, 20] frequency domain blind channel estimation methods using cross relations between antennas with a single OFDM block have been published. Methods that use single OFDM block are well suited for systems where the fast channel variations occur.

1.5 Aim and Outline of the Thesis

In this thesis, we are mainly interested in cyclic prefix based time and frequency domain blind channel estimation methods in SIMO-OFDM systems using only a single OFDM block. Our aim is to compare the performance of the time [18] and frequency domain [20] blind channel estimation methods with a reference system that knows the true channel characteristics.

Chapter 1 starts with an introduction to mathematical representation of OFDM. Also, OFDM history and previous work related to the channel estimation methods are given in this chapter.

In Chapter 2, system model is described with derivation of time and frequency domain blind channel estimation methods using cross relations between antennas as summarized from the papers of Wang, Lin & Chen, 2003 [18] and Park, Chun & Jeong, 2013 [20]. Receiver structure is explained with frequency domain equalizers and the ML estimator. Finally, information about generating correlated channels is given.

In Chapter 3, our simulation results for time and frequency domain blind channel estimation methods are presented using different channel parameters. Effects of the channel length, number of subcarriers, receiver antenna diversity, modulation type (QPSK and 16-QAM), equalizer type (MMSE and ZF) and correlation between channels are observed on the time or frequency domain estimation methods. Comments related to these results are also given in this chapter.

Chapter 4 is devoted to the conclusion and discussion of the results on blind channel estimation methods.

Appendices are added to the end of the thesis explaining the relevant information.

CHAPTER 2

BLIND CHANNEL ESTIMATION METHODS FOR OFDM

2.1 Introduction

In this chapter, blind channel estimation methods and the related components used for SIMO-OFDM systems are discussed. In Section 2.2, SIMO-OFDM system model and related OFDM equations are given. Sections 2.3.1 describes the cross relation based time domain blind channel estimation method as explained by Wang *et al.* in [18]; and Section 2.3.2 summarizes the frequency domain estimation from the paper of Park *et al.* [20]. Section 2.4 describes the SIMO-OFDM receiver antenna structure. Filter coefficients of frequency domain zero forcing and minimum mean squared error equalizers are explained in Section 2.5.1 & 2.5.2 respectively. Maximum likelihood criterion used in the receiver antenna structure is defined in Section 2.6. Channel envelope correlation and generation of correlated channels are explained in Sections 2.7 & 2.8 respectively.

2.2 System Model

In this thesis, we consider a SIMO-OFDM system with 1 transmit, M_r receive antennas and N subcarriers, which is derived from the MIMO-OFDM system in Figure 2.1 with M_t=1 transmit antennas.

Using the m_t^{th} antenna, the Nx1 symbol vector $\boldsymbol{s}_{m_t} = [s_{m_t}(1), s_{m_t}(2), ..., s_{m_t}(N)]^T$ is transmitted with an assumption that $\mathbf{E}[|s_{m_t}(n)|^2] = 1$ for n=1, 2, ..., N, where $(\mathbf{.})^T$ and $\mathbf{E}[\mathbf{.}]$ denotes transpose of a matrix and the expectation operator respectively.

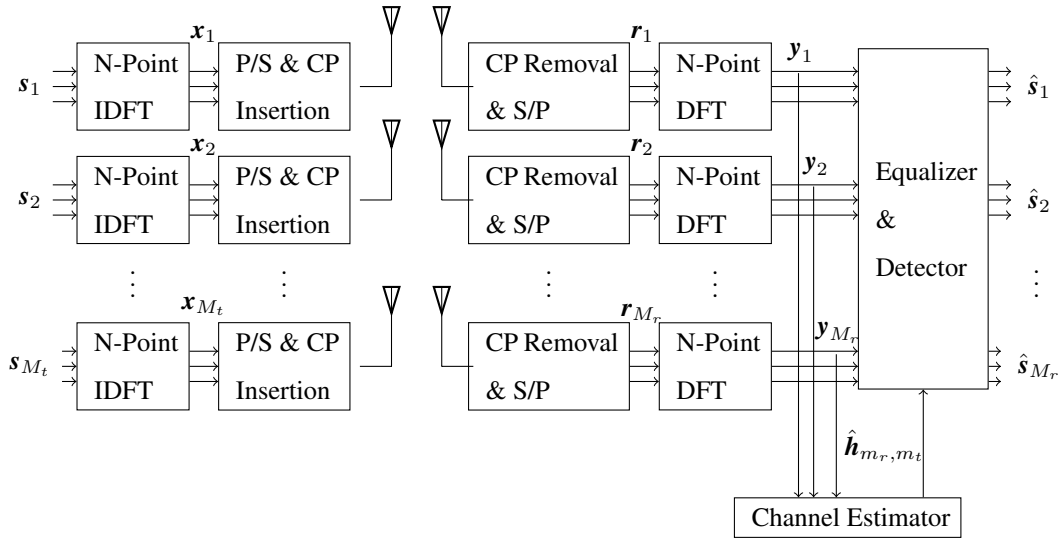

Figure 2.1: MIMO-OFDM block diagram [20]

Discrete Fourier Transform (DFT) matrix $\boldsymbol{W}_N \in \mathbb{C}^{N\times N}$ is used for matrix calculation in order to take Fourier Transform. The $(n,k)^{th}$ matrix element of $\boldsymbol{W}_N$ is shown as

$$W_{nk} = \frac{1}{\sqrt{N}}(\exp(-j2\pi/N))^{(n-1)(k-1)} \text{ for } 1\leq n,k \leq N$$

For the ease of notation, the normalizing factor $\frac{1}{\sqrt{N}}$ is used in above equation. Taking *N*-point Inverse Discrete Fourier Transform (IDFT) of $\boldsymbol{s}_{m_t}$, time domain OFDM symbol vector $\boldsymbol{x}_{m_t}$ is obtained as

$$\boldsymbol{x}_{m_t} = \boldsymbol{W}_N^H \boldsymbol{s}_{m_t}$$

where $\boldsymbol{x}_{m_t} = [x_{m_t}(1), x_{m_t}(2), ..., x_{m_t}(N)]^T$ and $(.)^H$ denotes the conjugate transpose of a matrix.

In order to remove Intersymbol Interference (ISI), cyclic prefix of length C_p, which is greater than the channel length L, is added to time domain symbol vector $\boldsymbol{x}_{m_t}$ and $\boldsymbol{x}'_{m_t}$ is obtained as

$$\boldsymbol{x}'_{m_t} = [x_{m_t}(N-C_p+1), x_{m_t}(N), x_{m_t}(1), ..., x_{m_t}(N)]^T$$

For the case where M_t transmitted signals are received through M_r antennas, time domain signal received through m_r^{th} antenna after cyclic prefix is taken out can be represented as

$$\boldsymbol{r}_{m_r} = \sum_{m_t=1}^{M_t} \boldsymbol{x}_{m_r} * \boldsymbol{g}_{m_r,m_t} + \boldsymbol{v}_{m_r} \tag{2.1}$$

where $\boldsymbol{g}_{m_r,m_t} = [g_{m_r,m_t}(0), g_{m_r,m_t}(1), ..., g_{m_r,m_t}(L-1)]^T$ is the channel impulse response between m_t^{th} transmit antenna and m_r^{th} receive antenna and $\boldsymbol{v}_{m_r} \in \mathbb{C}^{N\times 1}$ is a complex additive white Gaussian noise at the m_r^{th} antenna input. $(\boldsymbol{.})_{m_r,m_t}$ shows that, $(\boldsymbol{.})$ matrix belongs to m_t^{th} transmit and m_r^{th} receive antennas.

After DFT operation, frequency domain signal received through m_r^{th} antenna is obtained as

$$\hat{\boldsymbol{y}}_{m_r} = \boldsymbol{W}_N \boldsymbol{r}_{m_r} \tag{2.2}$$

$$\hat{\boldsymbol{y}}_{m_r} = \sum_{m_t=1}^{M_t} \boldsymbol{H}_{m_r,m_t} \boldsymbol{s}_{m_t} + \boldsymbol{z}_{m_r} = \boldsymbol{y}_{m_r} + \boldsymbol{z}_{m_r} \tag{2.3}$$

where $\boldsymbol{z}_{m_r}$ is the frequency domain noise vector represented as $\boldsymbol{z}_{m_r} = \boldsymbol{W}_N \boldsymbol{v}_{m_r}$ and $\boldsymbol{H}_{m_r,m_t}$ is a diagonal matrix that consists of diagonal entries of $\boldsymbol{h}_{m_r,m_t}$, where $\boldsymbol{h}_{m_r,m_t} = \boldsymbol{W}_L \boldsymbol{g}_{m_r,m_t} \in \mathbb{C}^{N\times 1}$ is the frequency response of the channel between m_t^{th} transmit antenna and m_r^{th} receive antenna, where $\boldsymbol{W}_L$ is the first L columns of $\boldsymbol{W}_N$.

2.3 SIMO-OFDM Blind Channel Estimation

In this section, two methods for SIMO-OFDM blind channel estimation are explained. For SIMO-OFDM case (M_t =1) the received signal equations can be written as

$$\hat{\boldsymbol{y}}_{m_r} = \boldsymbol{H}_{m_r,1} \boldsymbol{s}_1 + \boldsymbol{z}_{m_r} \tag{2.4}$$

2.3.1 Time Domain Method

In this subsection time domain method described by Wang, Lin & Chen [18] that is used for blind channel estimation is explained for one-transmitting, two-receiving antennas structure ($M_r = 2$).

For the noise free condition, received signals in the frequency domain can be written as

$$\boldsymbol{y}_1 = \boldsymbol{H}_{1,1} s_1$$

and

$$\boldsymbol{y}_2 = \boldsymbol{H}_{2,1} s_1$$

Equations for the n^{th} element ($1 \leq n \leq N$) of $\boldsymbol{y}_1$ and $\boldsymbol{y}_2$ can be written as

$$y_1(n) = s_1(n)\boldsymbol{h}_{1,1}(n) = s_1(n)\boldsymbol{w}_n\boldsymbol{g}_{1,1} \tag{2.5}$$

and

$$y_2(n) = s_1(n)\boldsymbol{h}_{2,1}(n) = s_1(n)\boldsymbol{w}_n\boldsymbol{g}_{2,1} \tag{2.6}$$

where n^{th} row of $\boldsymbol{W}_L$ is represented with $\boldsymbol{w}_n$ and the n^{th}element of the $\boldsymbol{h}_{m_r,1}$ is represented with $h_{m_r,1}(n)$.

Since $y_1(n), y_2(n), s_1(n), h_{1,1}(n)$ and $h_{2,1}(n)$ are all complex numbers, we can write an equation as

$$y_1(n)\boldsymbol{w}_n\boldsymbol{g}_{2,1} = y_2(n)\boldsymbol{w}_n\boldsymbol{g}_{1,1} \tag{2.7}$$

since

$$y_1(n)\boldsymbol{w}_n\boldsymbol{g}_{2,1} = s_1(n)\boldsymbol{w}_n\boldsymbol{g}_{1,1}\boldsymbol{w}_n\boldsymbol{g}_{2,1} = s_1(n)\boldsymbol{w}_n\boldsymbol{g}_{2,1}\boldsymbol{w}_n\boldsymbol{g}_{1,1} = y_2(n)\boldsymbol{w}_n\boldsymbol{g}_{1,1} \tag{2.8}$$

and equation can be written as subtraction equation

$$y_2(n)\boldsymbol{w}_n\boldsymbol{g}_{1,1} - y_1(n)\boldsymbol{w}_n\boldsymbol{g}_{2,1} = 0 \tag{2.9}$$

Equation becomes $\overline{\boldsymbol{Y}}\boldsymbol{g} = \boldsymbol{0}$, where $\overline{\boldsymbol{Y}} = [\tilde{\boldsymbol{Y}}_2\boldsymbol{W}_L - \tilde{\boldsymbol{Y}}_1\boldsymbol{W}_L] \in \mathbb{C}^{N\times 2L}$ with $\tilde{\boldsymbol{Y}}_{m_r}$ consisting of diagonal entries of $\boldsymbol{y}_{m_r}$, and $\boldsymbol{g} = [\boldsymbol{g}_{1,1}\ \ \boldsymbol{g}_{2,1}]^T \in \mathbb{C}^{2L\times 1}$.

In the noiseless case, Channel Impulse Response (CIR) matrix can be estimated up to a scalar ambiguity by solving homogeneous equation $\overline{\boldsymbol{Y}}\boldsymbol{g} = \boldsymbol{0}$. This homogenous equation can be solved using Singular Value Decomposition method. Solution of the $\boldsymbol{g}$ matrix will be the eigenvector corresponding to zero singular value of matrix $\overline{\boldsymbol{Y}}$.

For the noisy channel case above equation will not be equal to zero. So, we need to find matrix minimizing the equation below

$$\underset{\|\hat{\boldsymbol{g}}\|=1}{\arg\min}\, \hat{\boldsymbol{g}}^H\hat{\overline{\boldsymbol{Y}}}^H\hat{\overline{\boldsymbol{Y}}}\hat{\boldsymbol{g}} \tag{2.10}$$

where $\hat{\overline{\boldsymbol{Y}}} = [\tilde{\hat{\boldsymbol{Y}}}_2\boldsymbol{W}_L - \tilde{\hat{\boldsymbol{Y}}}_1\boldsymbol{W}_L] \in \mathbb{C}^{N\times 2L}$ with $\tilde{\hat{\boldsymbol{Y}}}_{m_r}$ that consists of diagonal entries of $\hat{\boldsymbol{y}}_{m_r}$ and $\hat{\boldsymbol{g}} = [\hat{\boldsymbol{g}}_{1,1}\ \ \hat{\boldsymbol{g}}_{2,1}]^T \in \mathbb{C}^{2L\times 1}$. For three and four receivers cases, the required $\hat{\overline{\boldsymbol{Y}}}$ matrices are explained in Appendix A.1.

CIR matrix can be estimated up to a scalar ambiguity using least-squares method. Solution of the $\hat{\boldsymbol{g}}$ matrix will be the eigenvector (right singular vector) corresponding to smallest singular value of $\hat{\overline{\boldsymbol{Y}}}$ matrix.

2.3.2 Frequency Domain Method

Frequency domain blind channel estimation method derived by Park, Chun & Jeong [20] can be divided into three steps; Antenna Relation Estimation, Subcarrier Relation Estimation and finding ambiguity factor.

For $M_r \geq 2$ we define new equation as

$$\overline{\boldsymbol{Y}}^{(M_r)}\boldsymbol{g} = \boldsymbol{0} \tag{2.11}$$

where $\overline{\boldsymbol{Y}}^{(M_r)}$ matrix contains $\tilde{\boldsymbol{Y}}_{m_r}$entries as shown below

$$\overline{\boldsymbol{Y}}^{(M_r)} = \begin{bmatrix} \tilde{\boldsymbol{Y}}_2\boldsymbol{W}_L & -\tilde{\boldsymbol{Y}}_1\boldsymbol{W}_L & & & & \\ \tilde{\boldsymbol{Y}}_3\boldsymbol{W}_L & \boldsymbol{0} & -\tilde{\boldsymbol{Y}}_1\boldsymbol{W}_L & & & \\ \vdots & \tilde{\boldsymbol{Y}}_3\boldsymbol{W}_L & -\tilde{\boldsymbol{Y}}_2\boldsymbol{W}_L & \ddots & & \\ \vdots & & & & \ddots & \\ \tilde{\boldsymbol{Y}}_{M_r}\boldsymbol{W}_L & \boldsymbol{0} & & & & -\tilde{\boldsymbol{Y}}_1\boldsymbol{W}_L \\ \boldsymbol{0} & & \overline{\boldsymbol{Y}}^{(M_r-1)} & \cdots & \cdots & \end{bmatrix} \in \mathbb{C}^{(N\times {}_{M_r}C_2)\times M_rL}$$

and

$$\boldsymbol{g} = \begin{bmatrix} \boldsymbol{g}_{1,1} \\ \boldsymbol{g}_{2,1} \\ \vdots \\ \boldsymbol{g}_{M_r,1} \end{bmatrix} \in \mathbb{C}^{(M_rL)\times 1}$$

with $\overline{\boldsymbol{Y}}^{(2)} = [\tilde{\boldsymbol{Y}}_2\boldsymbol{W}_L - \tilde{\boldsymbol{Y}}_1\boldsymbol{W}_L]$ and ${}_nC_k$ represents $\frac{n!}{k!(n-k)!}$. Using Discrete Fourier Transform matrix $\boldsymbol{W}_L$, $\boldsymbol{g}$ matrix in equation (2.11) can be replaced with $\boldsymbol{h}$ matrix (we use $\boldsymbol{Y}^{(M_r)}$ matrix instead of $\overline{\boldsymbol{Y}}^{(M_r)}$) then our equation can be reformulated as

$$\boldsymbol{Y}^{(M_r)}\boldsymbol{h} = \boldsymbol{0} \tag{2.12}$$

where

$$\boldsymbol{Y}^{(M_r)} = \begin{bmatrix} \tilde{\boldsymbol{Y}}_2 & -\tilde{\boldsymbol{Y}}_1 & & & & \\ \tilde{\boldsymbol{Y}}_3 & \boldsymbol{0} & -\tilde{\boldsymbol{Y}}_1 & & & \\ \vdots & \tilde{\boldsymbol{Y}}_3 & -\tilde{\boldsymbol{Y}}_2 & \ddots & & \\ \vdots & & & & \ddots & \\ \tilde{\boldsymbol{Y}}_{M_r} & \boldsymbol{0} & & & & -\tilde{\boldsymbol{Y}}_1 \\ \boldsymbol{0} & & \boldsymbol{Y}^{(M_r-1)} & \cdots & \cdots & \end{bmatrix} \in \mathbb{C}^{(N\times {}_{M_r}C_2)\times M_rN}$$

and

$$\boldsymbol{h} = \begin{bmatrix} \boldsymbol{h}_{1,1} \\ \boldsymbol{h}_{2,1} \\ \vdots \\ \boldsymbol{h}_{M_r,1} \end{bmatrix} \in \mathbb{C}^{(M_r N)\times 1}$$

with $\boldsymbol{Y}^{(2)} = [\tilde{\boldsymbol{Y}}_2 \quad -\tilde{\boldsymbol{Y}}_1]$. Since $\tilde{\boldsymbol{Y}}_{M_r}$ is a diagonal matrix, (2.12) can be split into subequations as

$$\boldsymbol{Y}^{(M_r)}(n)\boldsymbol{h}^s(n) = \boldsymbol{0} \text{ for } n = 1, ..., N \tag{2.13}$$

where

$$\boldsymbol{Y}^{(M_r)}(n) = \begin{bmatrix} y_2(n) & -y_1(n) & & & & \\ y_3(n) & 0 & -y_1(n) & & & \\ \vdots & y_3(n) & -y_2(n) & \ddots & & \\ \vdots & & & & \ddots & \\ y_{M_r}(n) & 0 & & & & -y_1(n) \\ \boldsymbol{0} & & \boldsymbol{Y}^{(M_r-1)}(n) & \cdots & \cdots & \end{bmatrix} \in \mathbb{C}^{(M_r C_2)\times M_r}$$

$$\boldsymbol{h}^{(s)}(n) = \begin{bmatrix} h^s_{1,1}(n) \\ h^s_{2,1}(n) \\ \vdots \\ h^s_{M_r,1}(n) \end{bmatrix} \in \mathbb{C}^{M_r\times 1}$$

Thus, up to a scalar ambiguity factor, the channel gains for each subcarrier can be estimated by solving (2.13) and we call this as Antenna Relation Estimation (ARE) step. However, N scalar ambiguities exist for all subcarriers in total. Notice that splitting (2.12) into (2.13) destroys the relation among the subcarriers. Accordingly we define a weight vector that represents the subcarrier relation

$$\boldsymbol{a} = [a_1, a_2, ..., a_N]^T$$

we obtain

$$\boldsymbol{h}_{m_r,1} = \boldsymbol{a} \odot \boldsymbol{h}'_{m_r,1}$$

where $\boldsymbol{h}'_{m_r,1} = [h^s_{m_r,1}(1), h^s_{m_r,1}(2), ..., h^s_{m_r,1}(N)]$ whose elements are taken from $\boldsymbol{h}^s(n)$ in (2.13). $\odot$ operator denotes the componentwise product of two vectors. We

define $\boldsymbol{W}_L^{\perp} \in \mathbb{C}^{(N-L)\times N}$ matrix whose rows are formed by orthogonal bases of the orthogonal subspace of $\boldsymbol{W}_L$, which can be calculated using *null* method and $\boldsymbol{W}_L$ matrix in MATLAB. Using orthogonality principle we obtain

$$\boldsymbol{W}_L^{\perp}\boldsymbol{h}_{m_r,1} = \mathbf{0} \text{ for } m_r = 1, ..., M_r$$

since $\boldsymbol{W}_L^{\perp}\boldsymbol{h}_{m_r,1} = \boldsymbol{W}_L^{\perp}\boldsymbol{W}_L\boldsymbol{g}_{m_r,1} = \mathbf{0}$ which leads to

$$[h^s_{m_r,1}(1)\boldsymbol{w}_1^{\perp}, h^s_{m_r,1}(2)\boldsymbol{w}_2^{\perp}, ..., h^s_{m_r,1}(N)\boldsymbol{w}_N^{\perp}]\boldsymbol{a} = \mathbf{0} \text{ for } m_r=1, ..., M_r \tag{2.14}$$

where $\boldsymbol{w}_n^{\perp}$ is the n^{th} column vector of $\boldsymbol{W}_L^{\perp}$.

Therefore, solving (2.14) we can estimate the weight vector $\boldsymbol{a}$ and we call this step as Subcarrier Relation Estimation (SRE) step. Then from (2.13) and (2.14), the channel for the m_r^{th} receive antenna can be formulated as

$$\boldsymbol{h}_{m_r,1} = \alpha_{ambiguity}\boldsymbol{a} \odot \boldsymbol{h}'_{m_r,1} \tag{2.15}$$

where $\alpha_{ambiguity}$ denotes a scalar ambiguity from (2.14).

For noisy case, equations in (2.13) and (2.14) will not be equal to zero. Solution of the homogenous least-squares equation is explained in details in Appendix B. The least-squares method can be applied for the noisy case modifying steps as follows

$$\hat{\boldsymbol{h}}^{(s)}(n) = \underset{\|\boldsymbol{h}^{(s)}(n)\|=1}{\arg\min}\ \boldsymbol{h}^{(s)}(n)^H\hat{\boldsymbol{Y}}(n)^H\hat{\boldsymbol{Y}}(n)\boldsymbol{h}^{(s)}(n) \tag{2.16}$$

$$\hat{\boldsymbol{a}} = \underset{\|\boldsymbol{a}\|=1}{\arg\min}\, \boldsymbol{a}^H\hat{\boldsymbol{U}}^H\hat{\boldsymbol{U}}\boldsymbol{a} \tag{2.17}$$

where

$$\boldsymbol{U} = \begin{bmatrix} \hat{h}^{(s)}_{1,1}(1)\boldsymbol{w}_1^{\perp}, ..., \hat{h}^{(s)}_{1,1}(N)\boldsymbol{w}_N^{\perp} \\ \hat{h}^{(s)}_{2,1}(1)\boldsymbol{w}_1^{\perp}, ..., \hat{h}^{(s)}_{2,1}(N)\boldsymbol{w}_N^{\perp} \\ \vdots \\ \hat{h}^{(s)}_{M_r,1}(1)\boldsymbol{w}_1^{\perp}, ..., \hat{h}^{(s)}_{M_r,1}(N)\boldsymbol{w}_N^{\perp} \end{bmatrix} \in \mathbb{C}^{M_r(N-L)\times N} \tag{2.18}$$

and

$$\hat{\boldsymbol{Y}}^{(M_r)}(n) = \boldsymbol{Y}^{(M_r)}(n) + \Delta\boldsymbol{Y}^{(M_r)}(n) \tag{2.19}$$

where $\Delta\boldsymbol{Y}^{(M_r)}(n)$ is generated using $\boldsymbol{z}_{m_r}$ in (2.4). The above formulation is based on a single OFDM block of the received signal, but for K multiple OFDM blocks

$\hat{\boldsymbol{Y}}_k(n)|_{k=1,\ldots K}$ (2.16) is modified as

$$\hat{\boldsymbol{h}}^{(s)}(n) = \underset{\|\boldsymbol{h}^{(s)}(n)\|=1}{\arg\min}\ \boldsymbol{h}^{(s)}(n)^H \mathbf{E}[\hat{\boldsymbol{Y}}(n)^H \hat{\boldsymbol{Y}}(n)] \boldsymbol{h}^{(s)}(n) \tag{2.20}$$

where $\mathbf{E}[\hat{\boldsymbol{Y}}(n)^H \hat{\boldsymbol{Y}}(n)]$ is a sample mean of $\hat{\boldsymbol{Y}}(n)^H \hat{\boldsymbol{Y}}(n)$ that is calculated over K multiple OFDM blocks, that is;

$$\mathbf{E}[\hat{\boldsymbol{Y}}(n)^H \hat{\boldsymbol{Y}}(n)] = \frac{1}{K} \sum_{k=1}^{K} \hat{\boldsymbol{Y}}_k(n)^H \hat{\boldsymbol{Y}}_k(n)$$

For three and four receivers cases, the required $\hat{\boldsymbol{Y}}(n)$ matrices are explained in Appendix A.2.

2.4 Receiver Antenna Structure

SIMO receiver antenna structures consist of three components; channel estimator, equalizer and estimator (demodulator). In this work, channel estimator, ZF (section 2.5.1) or MMSE (section 2.5.2) equalizer is used together with ML (section 2.6) estimator at the receiver antennas in order to estimate transmitted symbols.

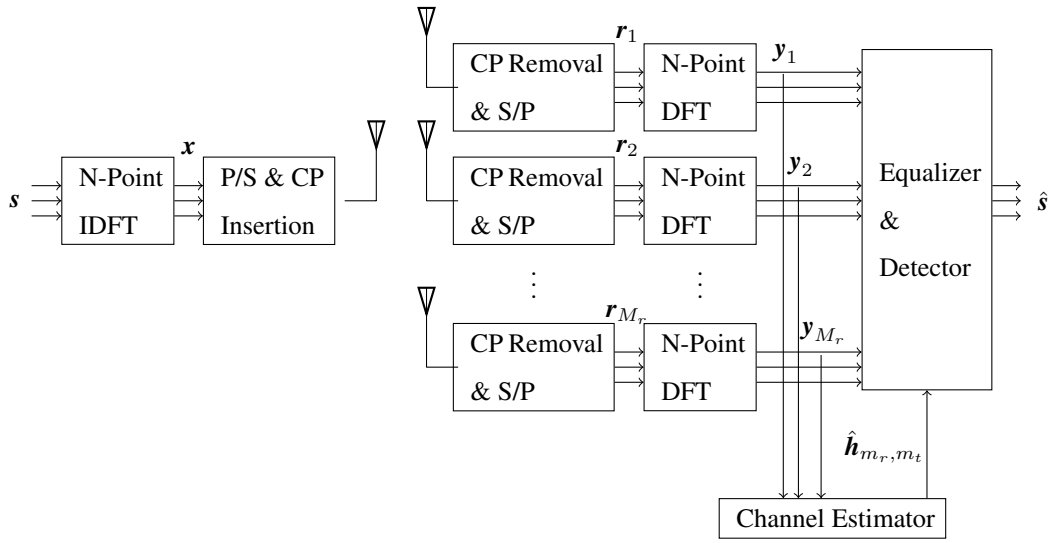

Figure 2.2: SIMO-OFDM block diagram

First of all, in order to obtain cross relations between channels, frequency domain signal vectors ($\hat{\boldsymbol{y}}_{m_r}$) are used in channel estimator. Matrices $\hat{\overline{\boldsymbol{Y}}}$ and $\hat{\boldsymbol{Y}}(n)$ used in the channel estimator are mentioned in Appendix A.

Secondly, estimated frequency domain channel vectors ($\hat{\boldsymbol{h}}_{m_r,m_t} = \boldsymbol{W}_L\hat{\boldsymbol{g}}_{m_r,m_t}$) are used in ZF or MMSE equalizers in order to equalize the received signal in frequency domain.

Finally the equalized signals are used in ML estimator to determine which symbol is transmitted.

2.5 Frequency Domain Equalization

Equalizers are used to mitigate the effects of the intersymbol interference. In this section we will define two linear frequency domain equalizers with low complexity as ZF and MMSE equalizers. Frequency domain equalizer structure is given in Figure 2.3. ZF and MMSE equalizers are explained in subsections 2.5.1 and 2.5.2 respectively.

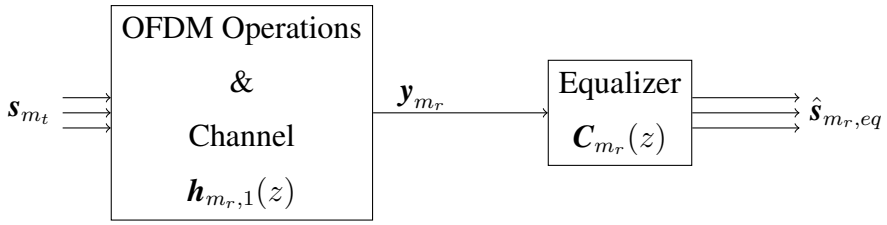

Figure 2.3: Frequency domain equalizer structure

2.5.1 Zero Forcing Equalizer

Zero Forcing equalizer is the simplest method for channel equalization used in the frequency domain. In the ZF equalizer, the received signal is assumed to be noiseless. Assuming $\boldsymbol{C}_{m_r}|_{ZF}(z)$ is the ZF equalizer filter used in the m_r^{th} antenna, $\boldsymbol{C}_{m_r}|_{ZF}(z)$ can be defined as the inverted frequency domain channel vector defined as

$$C_{m_r}|_{ZF}(n) = \frac{1}{\boldsymbol{h}_{m_r,1}(n)} \text{ for } n = 1, ..., N \text{ and } m_r = 1, ..., M_r \tag{2.21}$$

The equalized symbol at the ZF equalizer output can be simply calculated as

$$\hat{s}_{m_r,eq}(n) = \frac{y_{m_r}(n)}{\boldsymbol{h}_{m_r,1}(n)} \text{ for } n = 1, ..., N \text{ and } m_r = 1, ..., M_r \tag{2.22}$$

In the noisy case, small values of $h_{m_r,1}(n)$ cause noise enhancement in the equalized signal and reduces performance of the equalizer.

2.5.2 Minimum Mean Squared Error Equalizer

In MMSE equalizer, the tap weight coefficients $C_{m_r}|_{MMSE}(n)$ are adjusted to minimize the mean square value of the error

$$\boldsymbol{\epsilon} = \boldsymbol{s}_{m_t} - \hat{\boldsymbol{s}}_{m_r,eq}$$

where $\boldsymbol{s}_{m_t}$ is the transmitted symbol vector from the m_t^{th} transmitter antenna and $\hat{\boldsymbol{s}}_{m_r,eq}$ is the estimate of that symbol vector at the output of the equalizer at the m_r^{th} receiver antenna [21].

When the transmitted symbol vector $\boldsymbol{s}_{m_t}$ is complex-valued, the performance index for MMSE, denoted by J, is defined as [21]

$$\begin{aligned} J &= \mathbf{E}[\boldsymbol{\epsilon}]^2 \\ &= \mathbf{E}[\boldsymbol{s}_{m_t} - \hat{\boldsymbol{s}}_{m_r,eq}]^2 \end{aligned}$$

MMSE filter coefficients in the frequency domain are defined as

$$C_{m_r}|_{MMSE}(n) = \frac{\boldsymbol{h}^*_{m_r,1}(n)}{|\boldsymbol{h}_{m_r,1}(n)|^2 + \frac{1}{SNR}} \text{ for } n = 1, ..., N \text{ and } m_r = 1, ..., M_r \quad (2.23)$$

The equalized symbol at the MMSE equalizer output is calculated as

$$\hat{s}_{m_r}|_{MMSE}(n) = \frac{\boldsymbol{h}^*_{m_r,1}(n)}{|\boldsymbol{h}_{m_r,1}(n)|^2 + \frac{1}{SNR}} y_{m_r}(n) \text{ for } n = 1, ..., N \text{ and } m_r = 1, ..., M_r \quad (2.24)$$

2.6 Maximum Likelihood Estimator

The last component used in the receiver antenna structure is the ML estimator. For SIMO systems, transmitted symbols are determined using the outputs of each receiver antennas.

For the system defined in Figure 2.2 transmitted symbols are determined using the equalizer outputs of each receive antennas with ML criterion is defined as

$$\hat{s}(n) = \arg\min_{\overline{s} \in \mathbb{A}_s} \sum_{m_r=1}^{M_r} |\hat{s}_{m_r,eq}(n) - \overline{s}|^2 \text{ for } m_r = 1, ..., M_r \text{ and } n = 1, ..., N \quad (2.25)$$

where $\mathbb{A}_s$ is the set of all possible transmitted symbols.

The symbol $\overline{s}$, that minimizes the result of the summation is chosen as the estimated symbol at the output of ML estimator and is used for the calculation of bit error ratios.

2.7 Channel Envelope Correlation

This section describes determining the channel correlation using a Rayleigh fading channel model with the local scattering in a multiple case system, which has been proposed by Salz and Winters [22] and mentioned in PhD thesis by A. Yanartas [23].

In the channel model, a linear array is employed at the receiver, which consists of M_r identical elements, each giving the same response for any given direction.

Consider the first antenna be the reference on the array and the array response vector be given by

$$\boldsymbol{R}_a(\theta) = [1 \;\; e^{j2\pi d_1 sin\theta} \;\; e^{j2\pi d_2 sin\theta} \;\; \cdots \;\; e^{j2\pi d_{M_r-1} sin\theta}]^T \tag{2.26}$$

where θ is the angle between the arriving signal and the normal to the array and d_{m_r-1} is the distance between 1^{st} and m_r^{th} antennas in terms of the wavelength λ for m_r = 1, ..., M_r.

Figure 2.4 shows a typical scenario of a mobile radio propagation, assuming that the signals arrive from mobile to base station within an interval [-Δ, Δ] referred to as angle spread, centered at the angle of θ.

The correlation matrix of the array response vector $\boldsymbol{R}_a(\theta)$ is defined as

$$\sum_{\boldsymbol{R}_a} = \mathbf{E}[\boldsymbol{R}_a(\theta)\boldsymbol{R}_a(\theta)^H]$$

Real and imaginary parts of $(i,j)^{th}$ element of $\sum_{\boldsymbol{R}_a}$ is given by

$$Re\Big[\sum_{\boldsymbol{R}_a}(i,j)\Big] = J_0(d_{i,j}) + 2\sum_{k=1}^{\infty} J_{2k}(d_{i,j}) cos(2k\theta)\frac{sin(2k\Delta)}{2k\Delta} \tag{2.27}$$

$$Im\Big[\sum_{\boldsymbol{R}_a}(i,j)\Big] = 2\sum_{k=0}^{\infty} J_{2k+1}(d_{i,j}) sin((2k+1)\theta)\frac{sin((2k+1)\Delta)}{(2k+1)\Delta} \tag{2.28}$$

where J_0 is the Bessel function of zero order and $d_{i,j}$ is the distance between i^{th} and j^{th} antennas given as $d_{i,j} = 2\pi(d_i - d_j)$. Detailed derivations are explained in [22,23].

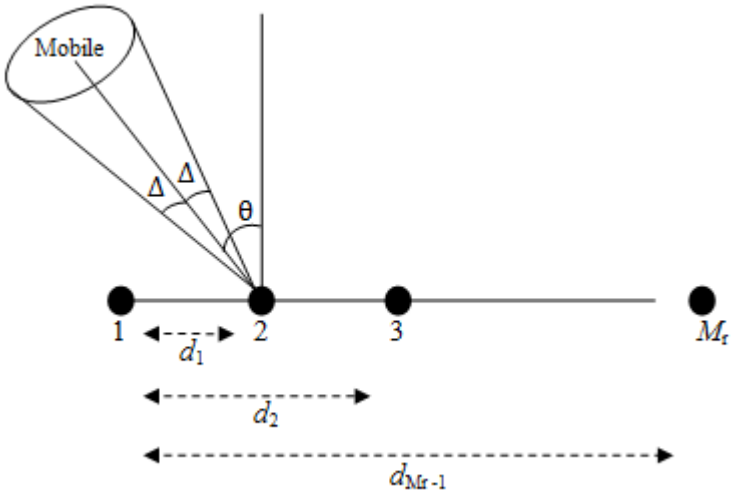

Figure 2.4: Wireless environment where all signals from mobile arrive at base station within $\pm\Delta$ at angle θ [22, 23]

The envelope correlation is $\eta_{\boldsymbol{R}_a}(i,j)$ defined as

$$\eta_{\boldsymbol{R}_a}(i,j) = \sqrt{\left(Re\left[\sum_{\boldsymbol{R}_a}(i,j)\right]\right)^2 + \left(Im\left[\sum_{\boldsymbol{R}_a}(i,j)\right]\right)^2} \tag{2.29}$$

Figure 2.5 shows the envelope correlation versus antenna spacing graph for $\theta = 0^\circ$ and $\Delta = 20^\circ$. Envelope correlation can be determined using the d/λ according to the given figure for $\theta = 0^\circ$ and $\Delta = 20^\circ$.

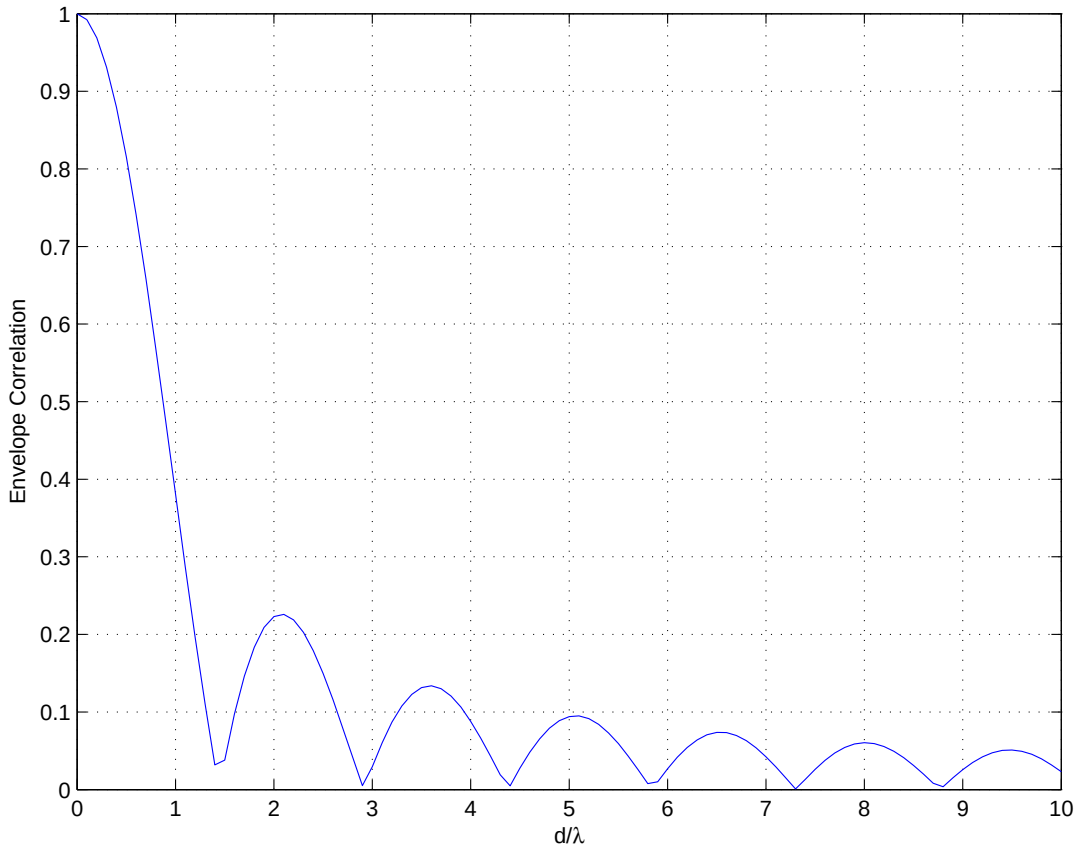

Figure 2.5: Correlation versus antenna spacing for $\theta = 0°$ and $\Delta = 20°$

2.8 Generation of Correlated Channels

In Section 2.2, $\boldsymbol{g}_{m_r,m_t}$ is defined as the channel impulse response between the m_t^{th} transmitting and m_r^{th} receiving antennas. Considering SIMO-OFDM systems, depending on the channel angle spread, the correlation coefficient between channels $\boldsymbol{g}_{i,1} = [g_{i,1}(0), ..., g_{i,1}(L-1)]^T$ and $\boldsymbol{g}_{j,1} = [g_{j,1}(0), ..., g_{j,1}(L-1)]^T$ is determined as

$$\rho_{i,j} = \frac{\mathbf{E}[g_{i,1}(l)g_{j,1}^*(l)]}{\sqrt{\mathrm{Var}(\boldsymbol{g}_{i,1})\mathrm{Var}(\boldsymbol{g}_{j,1})}} \quad \forall l \tag{2.30}$$

where l denotes the time index of the channel impulse response; $\mathbf{E}[.]$ and $\mathrm{Var}(.)$ denote the expected value and the variance respectively. The correlation coefficient ($\rho_{i,j}$) is used in the correlation matrix in order to create the correlated channels.

The correlated channels are generated by multiplying the uncorrelated channels with the matrix obtained from the Cholesky Decomposition of the desired correlation matrix ($\boldsymbol{C}_M$). To illustrate, lets say we have two complex uncorrelated channel impulse

responses as $\boldsymbol{g}_{1,1} \in \mathbb{C}^{L\times 1}$ and $\boldsymbol{g}_{2,1} \in \mathbb{C}^{L\times 1}$. The correlation matrix of these two channels is defined as

$$\boldsymbol{C}_M(\boldsymbol{g}_1, \boldsymbol{g}_2) = \begin{bmatrix} 1 & \rho_{1,2} \\ \rho_{1,2}^* & 1 \end{bmatrix} \in \mathbb{C}^{2\times 2} \tag{2.31}$$

The Cholesky Decomposition of the $\boldsymbol{C}_M$ is a decomposition of the form

$$\boldsymbol{C}_M = \boldsymbol{T}_M \boldsymbol{T}_M{}^* \tag{2.32}$$

where $\boldsymbol{T}_M$ is a lower triangle matrix with complex diagonal entries and $\boldsymbol{T}_M{}^*$ is the conjugate transpose of the $\boldsymbol{T}_M$. Note that, $\boldsymbol{C}_M$ should be a positive definite matrix for the Cholesky Decomposition.

The correlated channels $\ddot{\boldsymbol{g}}_1 \in \mathbb{C}^{L\times 1}$ and $\ddot{\boldsymbol{g}}_2 \in \mathbb{C}^{L\times 1}$ are created by multiplying the uncorrelated channels with the $\boldsymbol{T}_M{}^*$ matrix as

$$\begin{bmatrix} \ddot{\boldsymbol{g}}_1 & \ddot{\boldsymbol{g}}_2 \end{bmatrix} = \begin{bmatrix} \boldsymbol{g}_1 & \boldsymbol{g}_2 \end{bmatrix} \boldsymbol{T}_M{}^* \tag{2.33}$$

CHAPTER 3

SIMULATION RESULTS

3.1 Introduction

In this chapter, cross relation based time and frequency domain blind channel estimation methods are compared by using simulations conducted in MATLAB environment. Simulations are performed for different number of receiver antennas (M_r), channel lengths (L), number of subcarriers (N) using correlated and uncorrelated channel groups (channel pairs, triples or quadruples, depending on M_r).

Main computational cost for both estimation methods is the singular value decomposition. As mentioned in Park *et al.* [20], if Golub-Reinsch singular value decomposition is applied, ($16NL^2$+8) multiplications are needed for the time domain method. For the frequency domain method, steps of antenna relation estimation and subcarrier relation estimation need to be considered, which cost N and (N^2(16N - 8L+6) - $2NL$) computations respectively. Comparing dominant terms for both methods, the computation complexities of time and frequency domain methods are $O(NL^2)$ and $O(N^3)$ respectively.

In simulations, both correlated and uncorrelated channels are assumed to have Rayleigh fading distribution with exponentially decaying profile. QPSK or 16-QAM signaling is used for modulation. Through the simulations, the channel length (L) is assumed to be known by the receiver. In order to resolve the scalar ambiguity, we have assumed that the first gain ($g_{1,1}(0)$) of the first channel impulse response is known.

Mean Squared Error (MSE) and Normalized Root Mean Squared Error (NRMSE) results are obtained by averaging over a number of channel groups (N_{cg}) and Monte Carlo runs (M_c).

In order to estimate the symbols used for transmission, Minimum Mean Squared Error (MMSE) equalizers and Zero Forcing (ZF) equalizers are used together with Maximum Likelihood (ML) estimators in receiver antennas. Bit Error Ratios (BER) are calculated at the ML estimator outputs using the estimated symbols $\hat{\boldsymbol{s}}$. BER results are averaged over M_c Monte Carlo runs and N_{cg} channel groups.

Corresponding Mean Absolute Error (MAE), MSE and NRMSE values are calculated for time and frequency domain methods using the impulse responses $\boldsymbol{g}$ of length L and the corresponding frequency responses $\boldsymbol{h}$ of length N, in the set of N_{cg} channel groups as follows.

$$MAE_{time} = \frac{1}{N_{cg}} \sum_{i=1}^{N_{cg}} \frac{1}{M_c} \sum_{j=1}^{M_c} \sum_{l=1}^{L} |g_{2,1}^{(i)}(l) - \hat{g}_{2,1}^{(i,j)}(l)| \tag{3.1}$$

$$MSE_{time} = \frac{1}{N_{cg}} \sum_{i=1}^{N_{cg}} \frac{1}{M_c} \sum_{j=1}^{M_c} \|\boldsymbol{g}^{(i)} - \hat{\boldsymbol{g}}^{(i,j)}\|^2 \tag{3.2}$$

$$NRMSE_{time} = \frac{1}{N_{cg}} \sum_{i=1}^{N_{cg}} \frac{1}{\|\boldsymbol{g}^{(i)}\|} \sqrt{\frac{1}{M_c} \sum_{j=1}^{M_c} \|\boldsymbol{g}^{(i)} - \hat{\boldsymbol{g}}^{(i,j)}\|^2} \tag{3.3}$$

$$MAE_{frequency} = \frac{1}{N_{cg}} \sum_{i=1}^{N_{cg}} \frac{1}{M_c} \sum_{j=1}^{M_c} \sum_{n=1}^{N} |h_{2,1}^{(i)}(n) - \hat{h}_{2,1}^{(i,j)}(n)| \tag{3.4}$$

$$MSE_{frequency} = \frac{1}{N_{cg}} \sum_{i=1}^{N_{cg}} \frac{1}{M_c} \sum_{j=1}^{M_c} \|\boldsymbol{h}^{(i)} - \hat{\boldsymbol{h}}^{(i,j)}\|^2 \tag{3.5}$$

$$NRMSE_{frequency} = \frac{1}{N_{cg}} \sum_{i=1}^{N_{cg}} \frac{1}{\|\boldsymbol{h}^{(i)}\|} \sqrt{\frac{1}{M_c} \sum_{j=1}^{M_c} \|\boldsymbol{h}^{(i)} - \hat{\boldsymbol{h}}^{(i,j)}\|^2} \tag{3.6}$$

Simulations are performed for SIMO OFDM blind channel and parameter estimations as follows. First, a channel group is generated, where the channels are either correlated or uncorrelated and the channels in this group are fixed for all SNR values and Monte Carlo simulations. Then, Monte Carlo simulations are performed and the

received signal in the frequency domain is simulated with either QPSK or 16-QAM modulation scheme for all SNR values. Using the received signals, the channels are estimated using blind time or frequency domain estimation methods. Moreover, frequency domain received signals and estimated channel vectors are used in ZF or MMSE equalizer with ML estimator to estimate transmitted symbols. Throughout the simulations, for each SNR values and Monte Carlo runs, new symbol and noise vectors are generated and at the end of each Monte Carlo simulations NRMSE and BER results are calculated. After the simulations are completed for the chosen channel group, the new channel group is generated and the simulations are repeated. While the simulations are in progress, all NRMSE and BER results are saved and at the end of simulations for N_{cg} channel groups, NRMSE and BER results are averaged over M_c Monte Carlo runs and the number of channel groups N_{cg}.

Equations (3.2) & (3.5) are used in Section 3.2 to compare the MSE results of the time and frequency domain estimation methods with the ones plotted in [20].

When channel coefficients in the time domain have very small magnitudes, blind channel estimation may yield unreasonable results especially at low SNR's, and the MSE averaged over N_{cg} channels [18] given by equations (3.2) & (3.5) may be extremely dominated by the large-valued MSE terms corresponding to that single channel. On the other hand, the square rooting operation of the NRMSE defined by equations (3.3) & (3.6) as in [24] makes a smoothing affect on the MSE and reduces the effect of unreasonably high terms as depicted in Appendix C. For that reason, we prefer the NRMSE measure over MSE as a more reliable performance criterion.

Simulations of this chapter are presented in three sections. In Section 3.2, MAE and MSE results are given for SIMO-OFDM with one-transmitting and two-receiving antennas. In Section 3.3, SIMO-OFDM blind channel estimation results are plotted for different number of receiving antennas, M_r=2, 3, 4; number of subcarriers N=16, 64 and the channel length L=3, 4, 5 using uncorrelated Rayleigh fading channels with QPSK and 16-QAM modulation schemes. In Section 3.4 the effect of the channel envelope correlation is investigated over time and frequency domain estimation methods and simulations are performed for different number of receiving antennas, M_r=2, 3, 4, using Rayleigh fading channels with QPSK modulation.

3.2 MAE and MSE Comparison Between Time and Frequency Estimation Methods

In this part, randomly generated uncorrelated Rayleigh fading channel pairs are used to compare the mean absolute error (MAE) and MSE results for time and frequency domain estimation methods in SIMO-OFDM with one-transmitting, two-receiving antennas. Both MAE and MSE values are calculated for the channels between the transmitting and the second receiving antennas ($\boldsymbol{g}_{2,1}$ or $\boldsymbol{h}_{2,1}$) as was done in [18]. However; in [18], the MAE values given by equations (3.1) and (3.4) are called 'bias', which is a mistake.

MAE is calculated using equations (3.1) and (3.4) for time and frequency domain methods respectively. MSE results are compared with the Cramér-Rao Bound (CRB).

Cramér-Rao Bound is a fundamental bound on the mean squared error of the unbiased estimator, which is firstly derived by H. Cramér [25] and C. R. Rao [26]. An unbiased estimator that achieves this bound is considered as efficient. CRB is used as a performance criterion for estimators and is calculated by taking the inverse of the Fisher information matrix. A detailed derivation of the Fisher information matrix can be found in Appendix D. To evaluate the CRB, we often consider one element of the channel ($g_{1,1}(0)$) is known. After deleting the columns and rows associated with the known parameter, CRB can be evaluated by inverting the remaining matrix [27].

In Figure 3.1 and Figure 3.2, we plot the mean absolute error (MAE) and MSE values respectively, obtained by time and frequency domain estimation methods for 50 randomly generated uncorrelated Rayleigh fading channel characteristics with parameters; sample time = 10^{-6} seconds, maximum Doppler shift = 100 Hz, path delay for $\boldsymbol{g}_{1,1}$ = [0, 1, 2, 3, 5]$\times 10^{-6}$ seconds, path delay for $\boldsymbol{g}_{2,1}$ = [0, 0.5, 1, 1.5, 2]$\times 10^{-6}$ seconds and average path gains [0, -3, -6, -9, -12] dB and [0, -2, -4, -6, -8] dB respectively.

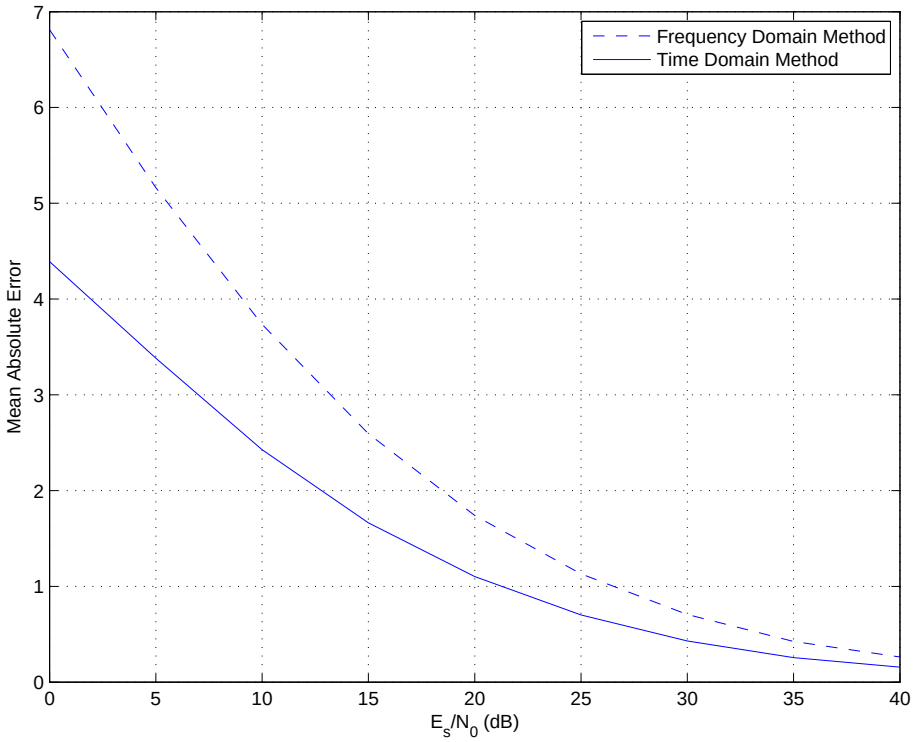

Figure 3.1: MAE of time and frequency domain methods for M_r=2, N=16, L=5, M_c=10^4, over 50 uncorrelated channel pairs with QPSK modulation

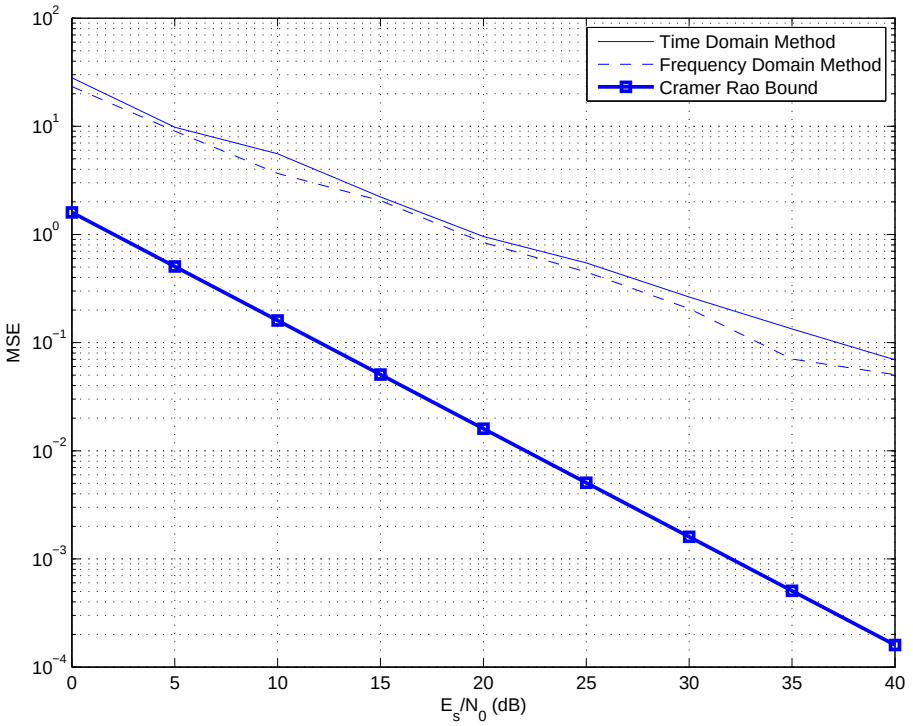

Figure 3.2: MSE of time and frequency domain methods for M_r=2, N=16, L=5, M_c=10^4, over 50 uncorrelated channel pairs with QPSK modulation

As it is seen from Figure 3.1 both methods are unbiased at high SNR. MAE values for the frequency domain method are greater than those of the time domain method. However, Park *et al.* claim in [20], that the MAE values of the frequency domain method are smaller. Although this is possible for a specific channel, we think that averages found over channel ensembles give more reliable information.

Although the MSE figure obtained for a specific channel in [20] shows that the results with time domain are better; our Figure 3.2 obtained by averaging over 50 random channel groups indicate slightly smaller MSE values for the frequency domain method at all SNR's.

3.3 Uncorrelated Channel Characteristics

In this section, cross relation based time and frequency domain blind channel estimation method results for SIMO-OFDM systems are given assuming uncorrelated channels with different number of channel lengths (L), subcarriers (N), receiving antennas (M_r), using different modulation schemes (QPSK or 16-QAM) and equalizers (ZF or MMSE).

In simulations, randomly generated channels are assumed to have Rayleigh fading distribution with exponentially decaying profile with parameters; sample time = 10^{-6} seconds, maximum Doppler shift = 100 Hz, path delays = [0 to 10]$\times 10^{-6}$ seconds and linearly decreasing average path gains. Mathematical model of Rayleigh fading channel is explained in Appendix E. Blind channel estimators are simulated using only a single OFDM block at each simulation. The output of the blind channel estimators are used at receivers with MMSE and ZF equalizers together with ML estimators in order to estimate the transmitted symbols.

The NRMSE values of the estimated channel characteristics and the BER of the estimated symbols are calculated for time and frequency domain estimations. In order to resolve the scalar ambiguity, it is assumed that the first gain of the first channel impulse response ($g_{1,1}(0)$) is known.

NRMSE values are calculated using equations (3.3) and (3.6) for time and frequency

domain methods respectively. As described in Section 3.1, assuming a known channel gain ($g_{1,1}(0)$) leads to unreasonable estimation results when channel coefficients in the time domain have a very small magnitude, which contributes a lot to the NRMSE and BER results. Hence, the results are averaged over a number of generated channel groups for each simulation.

3.3.1 Effect of the Channel Length

We first investigate the behaviour of time and frequency domain channel estimation methods with respect to the length of the channel impulse response.

SIMO OFDM with one-transmitting and two-receiving antennas is simulated using channel lengths L= 2 to 5, number of subcarriers N=16, cyclic prefix length (C_p)=5, MMSE Equalizer with ML estimator for 10^4 Monte Carlo runs and 50 uncorrelated channel groups. NRMSE and BER results are plotted for different SNR values in Figure 3.3 and Figure 3.4 for QPSK modulation scheme. Also, true channel BER results are plotted in BER comparison figures.

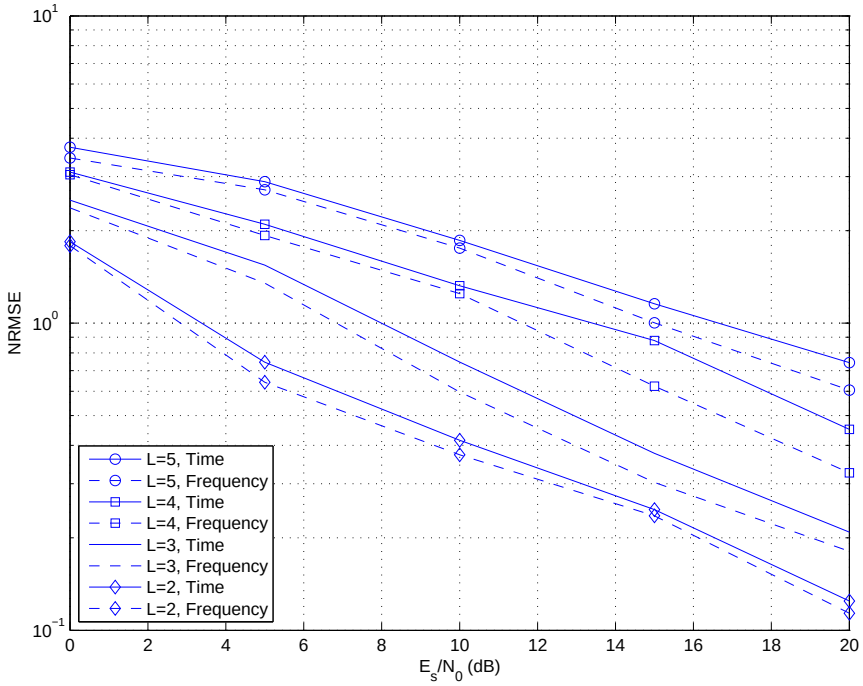

Figure 3.3: NRMSE of time and frequency domain methods for M_r=2, N=16, M_c=10^4, over 50 uncorrelated channel groups with QPSK modulation

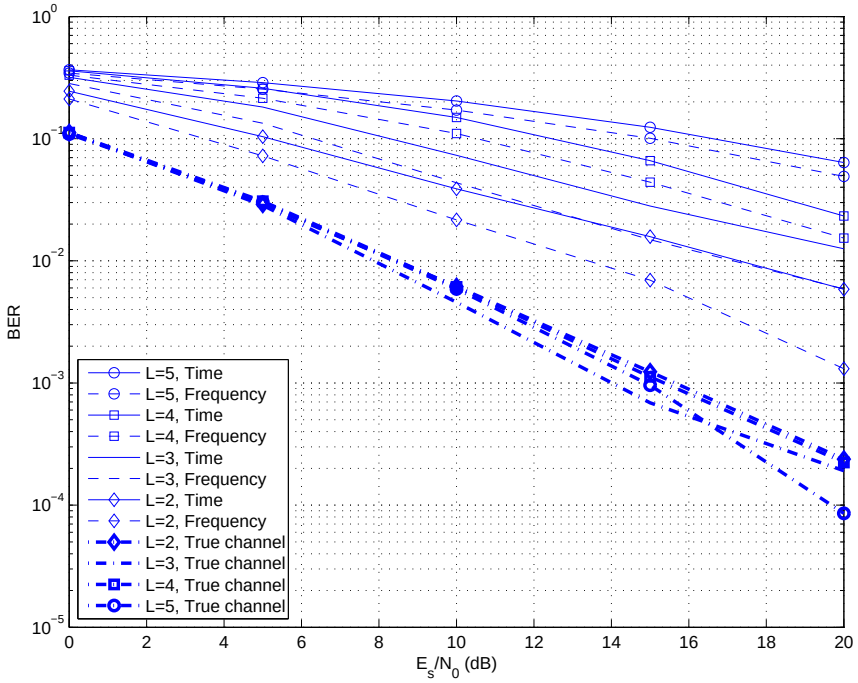

Figure 3.4: Probability of bit error for time and frequency domain methods for M_r=2, N=16, M_c=10^4, over 50 uncorrelated channel groups with QPSK modulation

From NRMSE and BER figures, it can be inferred that, an increase in the channel length L decreases the performance of the blind channel estimation. However, when compared with the true channel results, one can say that even for the best case, L=2, there is an SNR loss of 5 dB for the frequency and 9 dB for the time domain blind channel estimators, at BER=10^{-2}.

With QPSK modulation, frequency domain estimation results are slightly better than those of the time domain method. In [20] time and frequency domain method MSE results are compared for L=3, 4 and 5. Especially for L=4 and 5 cases, for the same MSE, respectively 15 dB and 20 dB more SNR is required for the time domain method, which disagree with our results.

3.3.2 Effect of the Number of Subcarriers

Secondly we try to observe the behaviour of the time and frequency domain estimation methods with respect to the number of subcarriers (N).

SIMO OFDM with one-transmitting, two-receiving antennas is simulated using

N=16 (with C_p=5), and N=64 (with C_p=16), MMSE Equalizer with ML estimator for 10^4 Monte Carlo runs and 50 uncorrelated channel groups. BER results are plotted in Figure 3.5 showing that an increase in the number of subcarriers increases the performance of blind channel estimation.

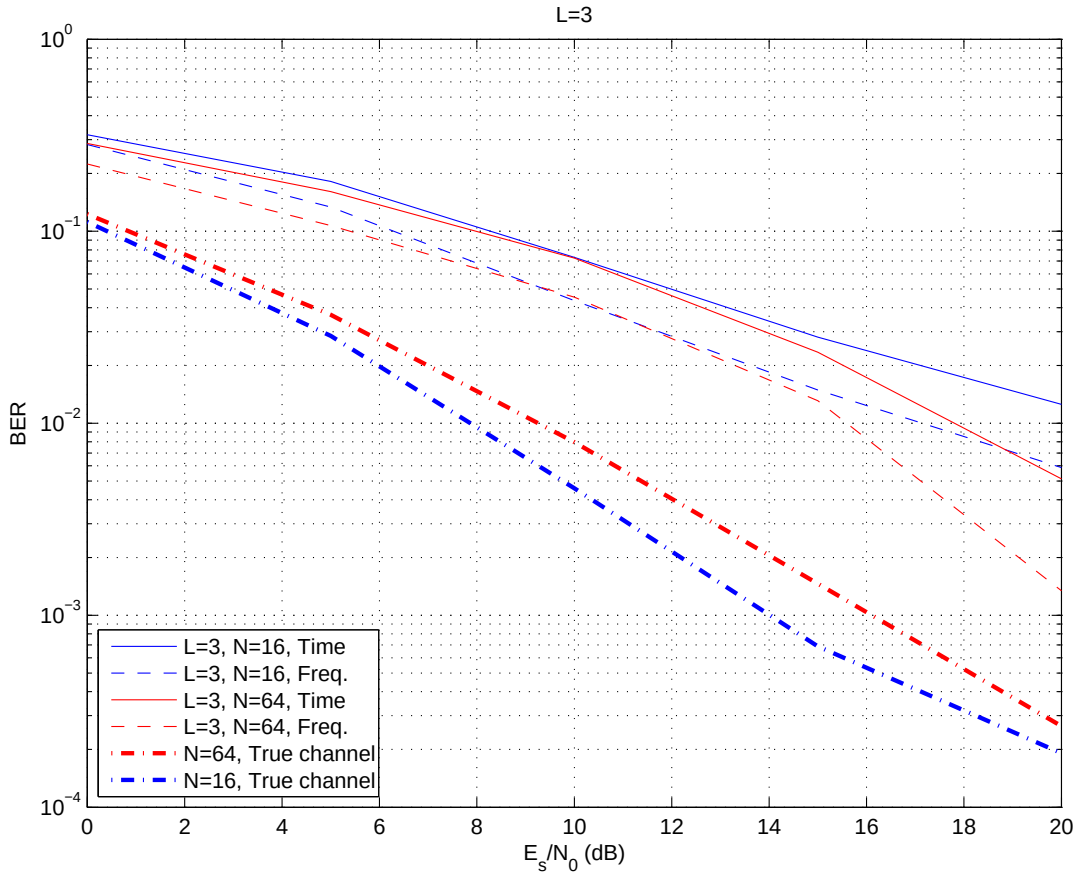

Figure 3.5: Probability of bit error for time and frequency domain methods with M_r=2, N=16 and 64, M_c=10^4, over 50 uncorrelated channel groups with QPSK modulation

Assuming perfect frequency synchronization, as the number of subcarriers are increased, more information is received about the channels through the frequency domain symbol vector ($\hat{\boldsymbol{y}}_{m_r}$) leading greater data matrices used in equation (2.10) for the time domain method and more cross relation functions in equation (2.16) for the frequency domain method. Thus, more information provides more successful blind channel estimations.

3.3.3 Effect of the Number of Receiving Antennas

In this part, we try to find the effect of receiver antenna diversity over blind channel estimation for 16 subcarriers and different channel lengths.

Figure 3.6 depicts the NRMSE values corresponding to 1x2, 1x3, 1x4 OFDM systems for L=3. In Figures 3.7 & 3.8 the length of the channel impulse response is chosen as L=4 and L=5 respectively.

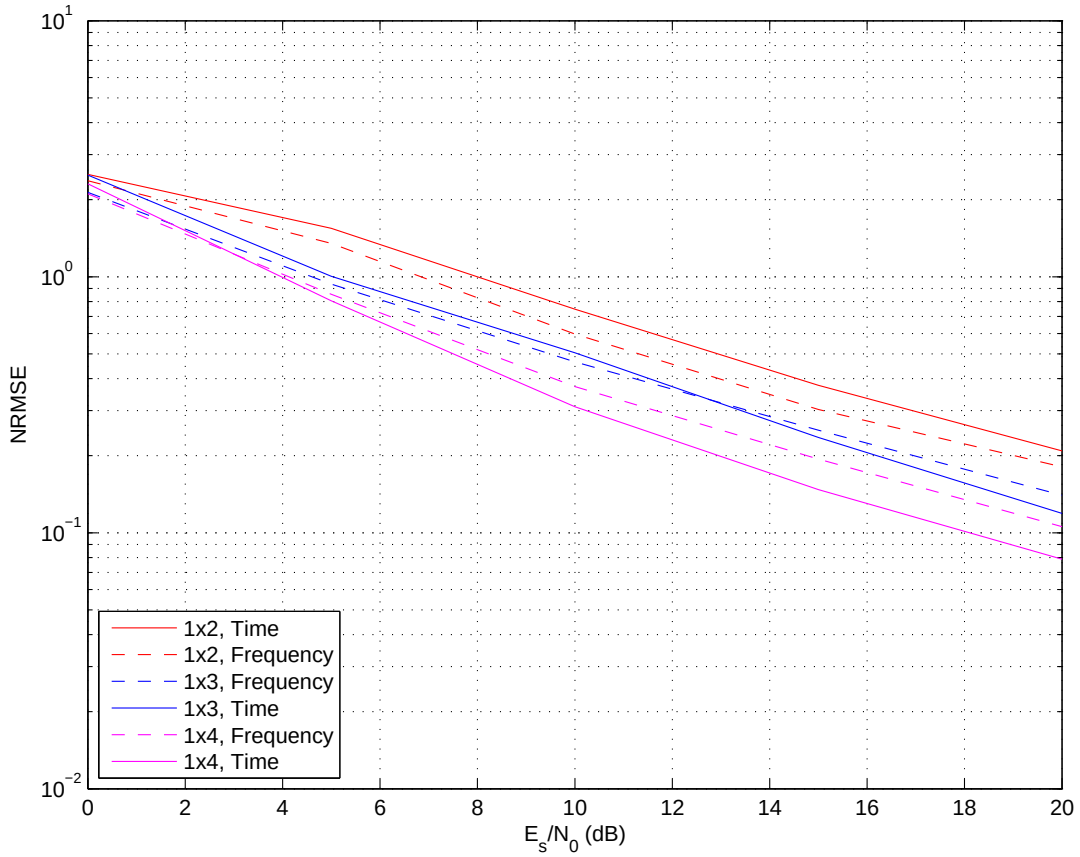

Figure 3.6: NRMSE of time and frequency domain methods for 1x2, 1x3 and 1x4 OFDM systems, N=16, $L = 3$, M_c=10^4, over 50 uncorrelated channel groups with QPSK modulation

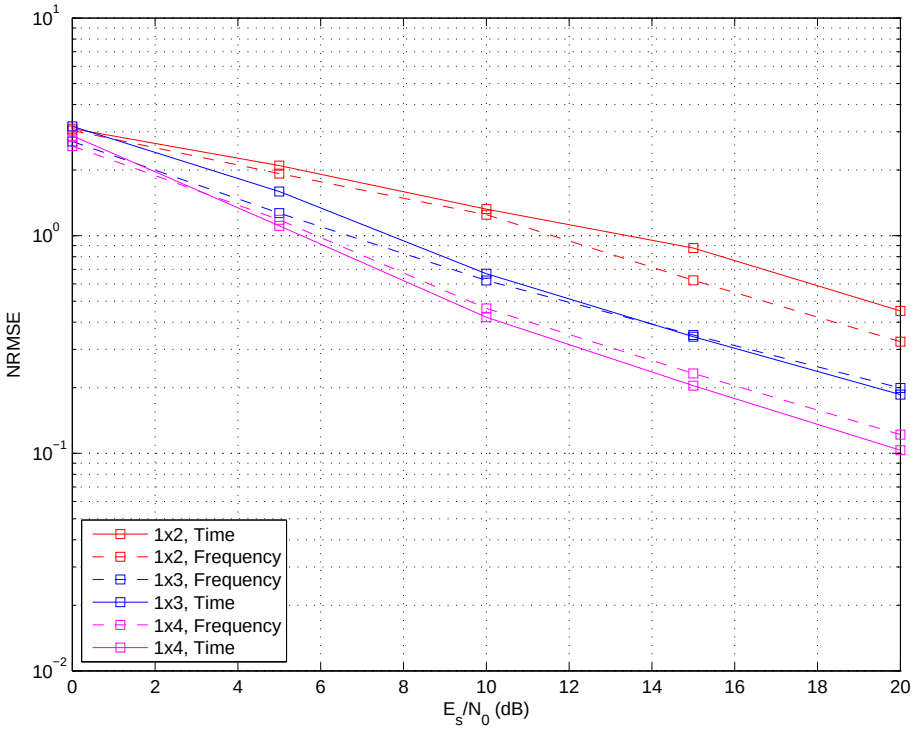

Figure 3.7: NRMSE of time and frequency domain methods for 1x2, 1x3 and 1x4 OFDM systems, N=16, $L = 4$, M_c=10^4, over 50 uncorrelated channel groups with QPSK modulation

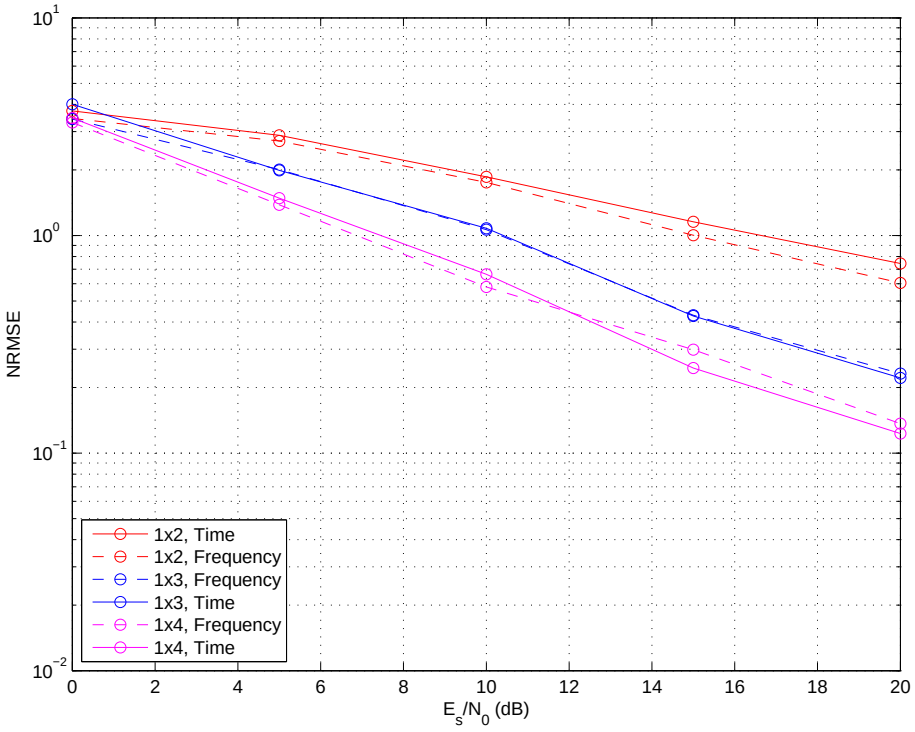

Figure 3.8: NRMSE of time and frequency domain methods for 1x2, 1x3 and 1x4 OFDM systems, N=16, $L = 5$, M_c=10^4, over 50 uncorrelated channel groups with QPSK modulation

It is observed that, increasing antenna diversity provides more information about the channels that results in better blind channel estimation.

Considering these three figures, frequency domain method seems to be superior to the time domain method. As the antenna diversity is increased, results of time domain method become better than those of the frequency domain method. Also the gaps between the NRMSE curves increase as the channel length increases.

Resulting BER curves are plotted in Figure 3.9, Figure 3.10 and Figure 3.11 respectively for $L = 3$, 4 and 5. MMSE equalizers and ML estimators are used in the receiver antennas.

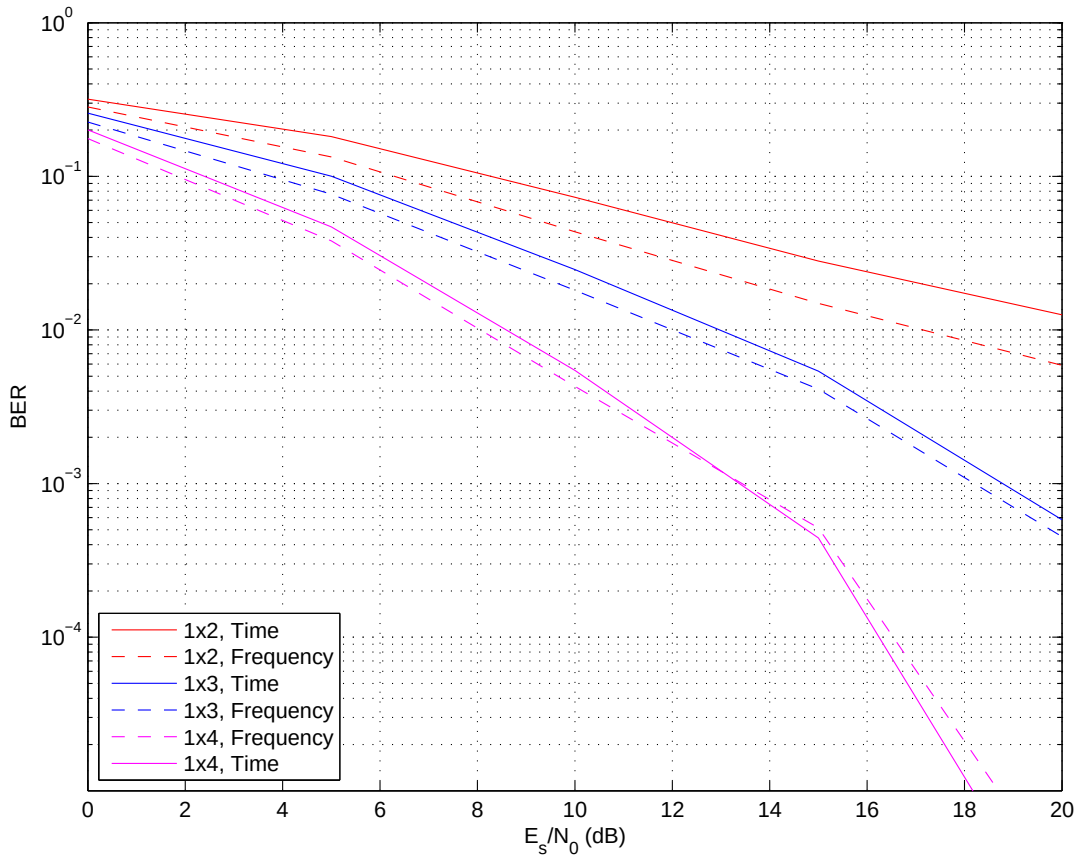

Figure 3.9: Probability of bit error for time and frequency domain methods for 1x2, 1x3 and 1x4 OFDM systems, $L = 3$, N=16, M_c=10^4, over 50 uncorrelated channel groups with QPSK modulation

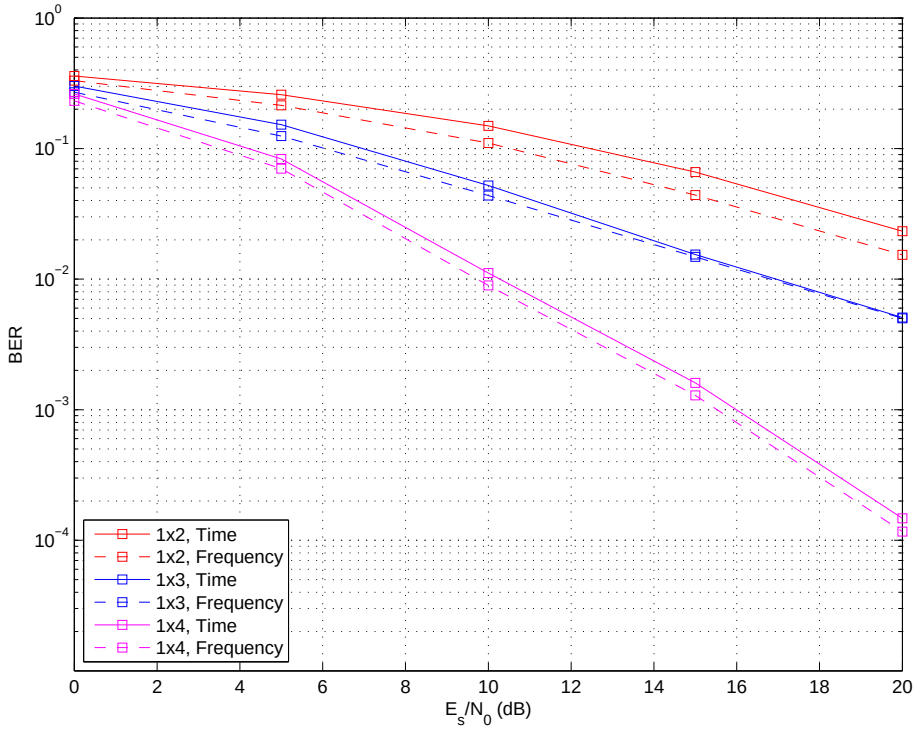

Figure 3.10: Probability of bit error for time and frequency domain methods for 1x2, 1x3 and 1x4 OFDM systems, $L = 4$, N=16, M_c=10^4, over 50 uncorrelated channel groups with QPSK modulation

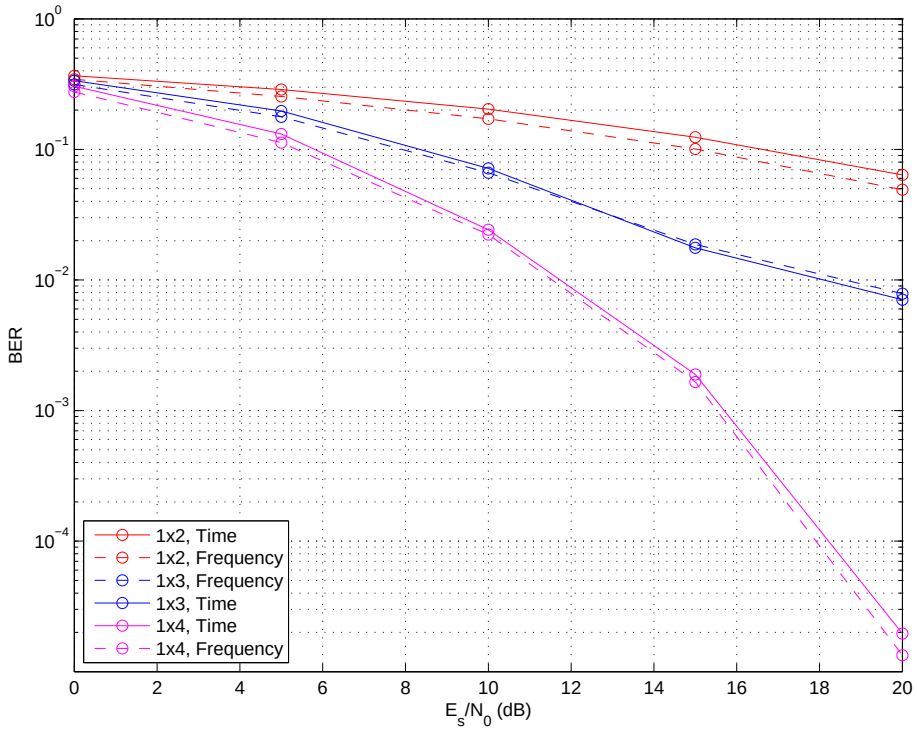

Figure 3.11: Probability of bit error for time and frequency domain methods for 1x2, 1x3 and 1x4 OFDM systems, $L = 5$, N=16, M_c=10^4, over 50 uncorrelated channel groups with QPSK modulation

In the BER figures, results are nearly the same for both time and frequency domain methods. By increasing the antenna diversity, more receiver outputs are used in ML estimators that increases the success rate at the estimating transmitted symbols. Increase in the antenna diversity reduces the required SNR to achieve the same BER. Taking BER=10^{-1} as a reference bit error probability, SNR results are summarized in Table 3.1.

Table 3.1: SNR differences at BER=10^{-1} using antenna diversity

SIMO OFDM Systems	1x2	1x3	1x4	Difference Between 1x2 and 1x3	Difference Between 1x3 and 1x4
L=3	6-8 dB	4-5 dB	2 dB	2-3 dB	2-3 dB
L=4	11-12 dB	6-7 dB	4-5 dB	5 dB	2 dB
L=5	15-17 dB	8 dB	6 dB	7-9 dB	2 dB

3.3.4 QPSK versus 16-QAM

In this section, we compare the effect of choosing QPSK or 16-QAM modulation over the blind estimation by means of the NRMSE and BER results for N=16 and L=4.

Figure 3.12 shows the NRMSE results obtained using time domain estimation method in SIMO OFDM systems. QPSK and 16-QAM modulation results are compared using N=16, L=4, 10^4 Monte Carlo runs and 50 uncorrelated Rayleigh fading channel groups.

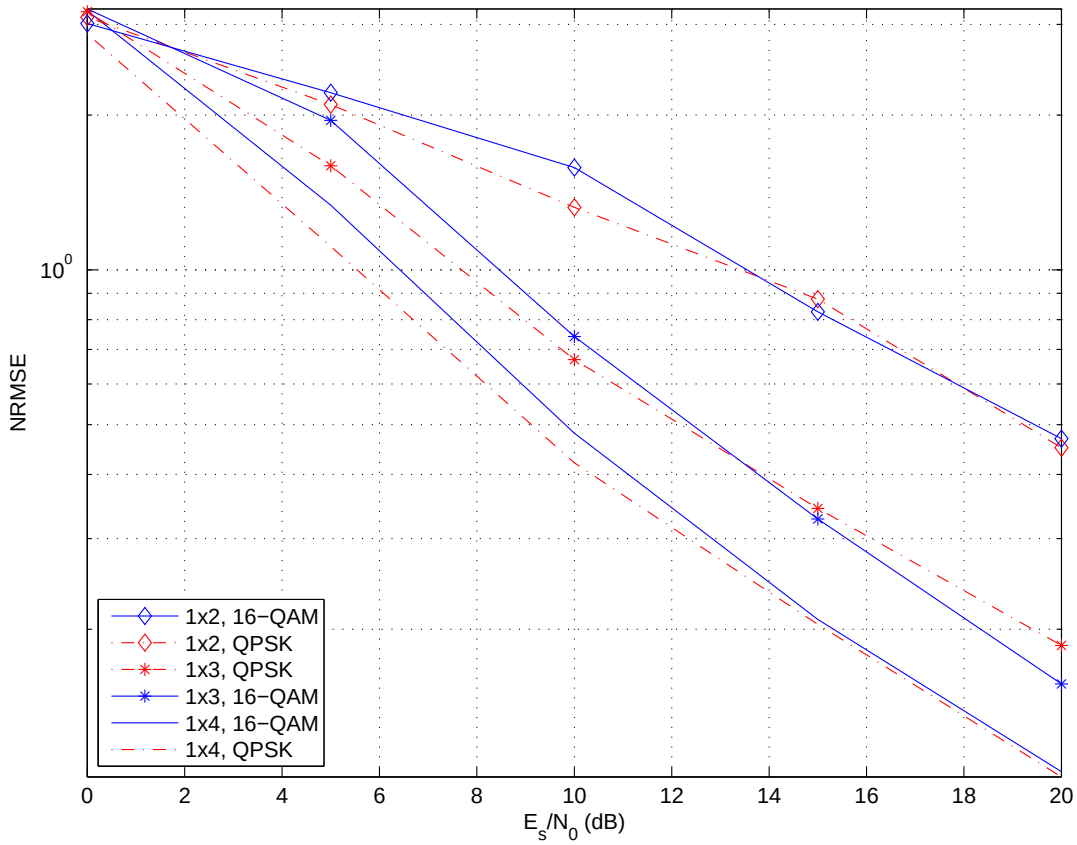

Figure 3.12: NRMSE of QPSK and 16-QAM modulation schemes for OFDM systems, $L = 4$, N=16, M_c=10^4, over 50 uncorrelated channel groups, using only the time domain method

It is inferred from Figure 3.12 that, the NRMSE performance of the time domain blind channel estimation is not affected from the modulation choice between QPSK and 16-QAM.

Figure 3.13 shows the bit error results for OFDM with one-transmitting, two-receiving antennas having MMSE equalizer and ML estimator at the receivers. QPSK and 16-QAM results are compared using N=16, L=4, 10^4 Monte Carlo runs and 50 uncorrelated Rayleigh fading channel groups. Symbol energies are normalized to one for QPSK and 16-QAM modulation schemes. In Figures 3.14 & 3.15, simulations are performed for 1x3 and 1x4 OFDM systems respectively, with the same parameters.

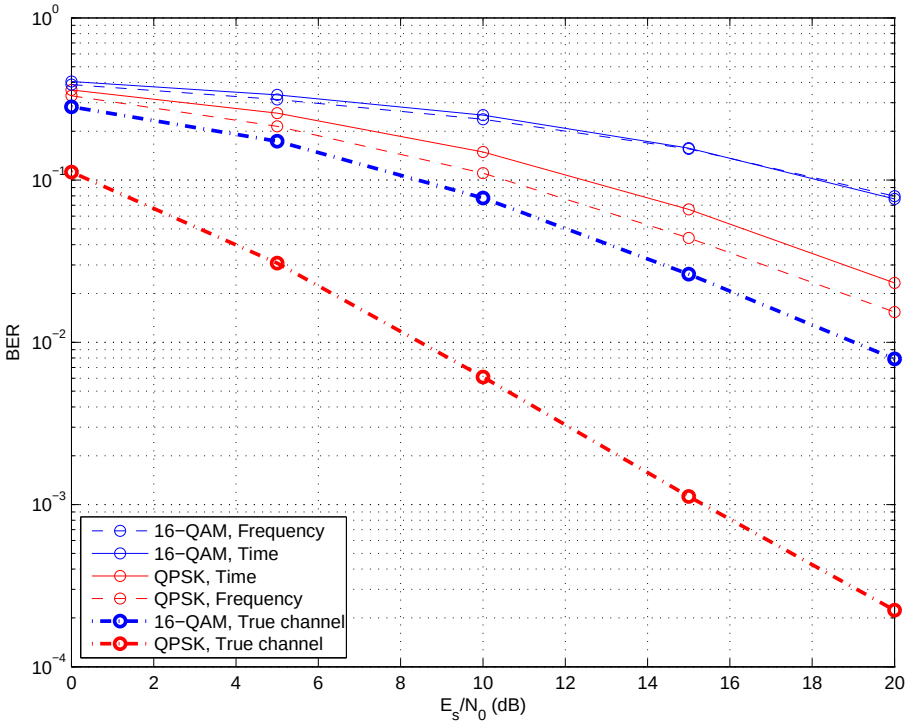

Figure 3.13: Probability of bit error for QPSK and 16-QAM modulations for 1x2 OFDM, $L = 4$, N=16, M_c=10^4, over 50 uncorrelated channel groups

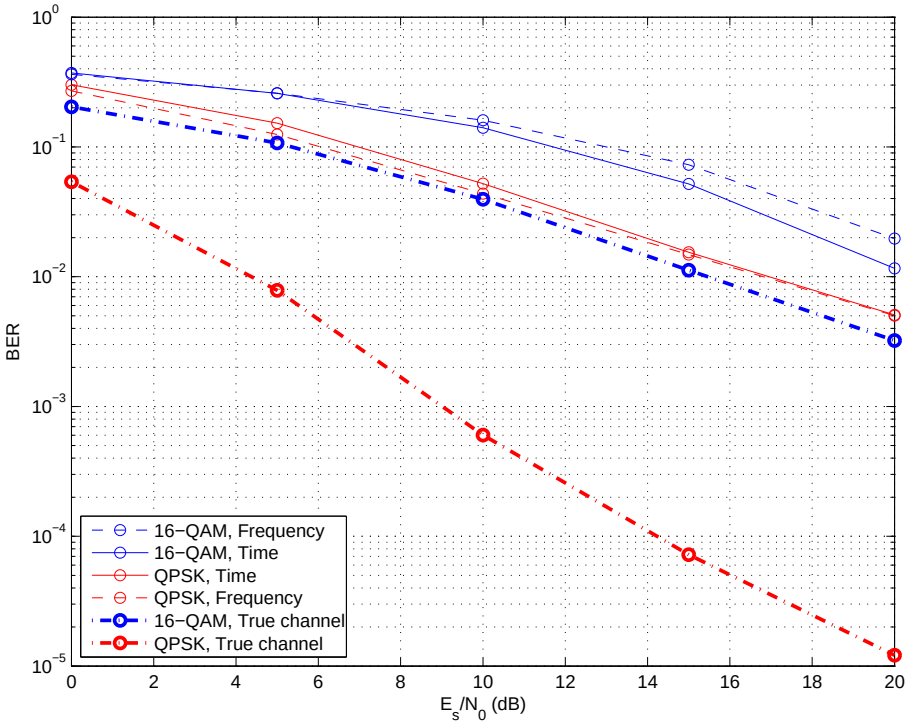

Figure 3.14: Probability of bit error for QPSK and 16-QAM modulations for 1x3 OFDM, $L = 4$, N=16, M_c=10^4, over 50 uncorrelated channel groups

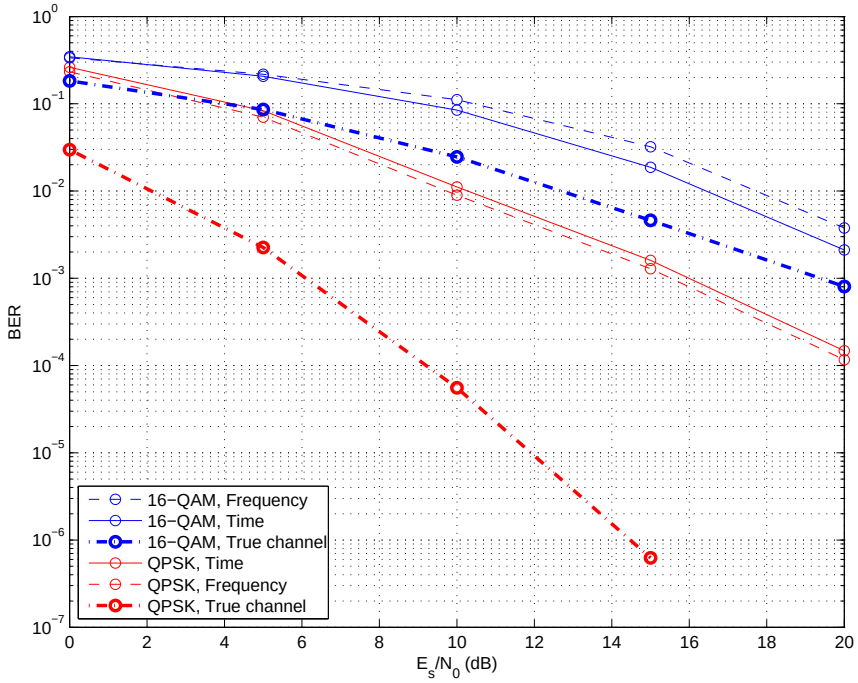

Figure 3.15: Probability of bit error for QPSK and 16-QAM modulations for 1x4 OFDM, $L = 4$, N=16, M_c=10^4, over 50 uncorrelated channel groups

From Figures 3.13, 3.14 & 3.15, one observes that QPSK modulation performs better than 16-QAM, as expected. At the same signal power, distances between symbols are smaller in the 16-QAM constellation causing reduction in the bit error rate performance.

If we compare the time and frequency domain blind channel estimations with the true channel results, although the estimation in the 16-QAM case yields slightly smaller losses than QPSK, considering both modulation schemes, the SNR loss is more than 10 dB for the 1x2 OFDM system at BER=10^{-1}, more than 6.5 dB for 1x3 OFDM system at BER=10^{-1}, and more than 4 dB for the 1x4 OFDM system at BER=10^{-2}. In Table 3.2, we summarize these SNR losses, which all seem to be excessively high and may be practically preferable only when the number of receiving antennas is more than 4.

In Figure 3.15, one may also observe that although there is no appreciable difference, time domain blind channel estimation seems to perform better than frequency domain estimation for 16-QAM (almost 1.5 dB gain at BER=10^{-2}); whereas time domain estimation is slightly worse than frequency domain estimation for QPSK (less than

0.5 dB loss at BER=10^{-2}).

Table 3.2: SNR losses with respect to the true channel

	QPSK		16-QAM	
	Freq.	Time	Freq.	Time
1x2 OFDM with BER=10^{-1}	10 dB	12 dB	10 dB	10 dB
1x3 OFDM with BER=10^{-1}	8 dB	9 dB	7.5 dB	6.5 dB
1x4 OFDM with BER=10^{-2}	∼8 dB	∼8 dB	∼5.5 dB	4 dB

3.3.5 ZF Equalizer versus MMSE Equalizer

In this part, we compare the BER results of the time and frequency domain blind channel estimation methods using either Zero Forcing (ZF) or Minimum Mean Squared Error (MMSE) equalizers explained in Section 2.5.1 and Section 2.5.2 respectively. Before this section, only the MMSE equalizer outputs are plotted in BER figures.

Figure 3.16 shows the BER results obtained using MMSE and ZF equalizers with the ML estimator for 1x2 OFDM having N=64, L=4, M_c=10^4 over 50 uncorrelated channel groups.

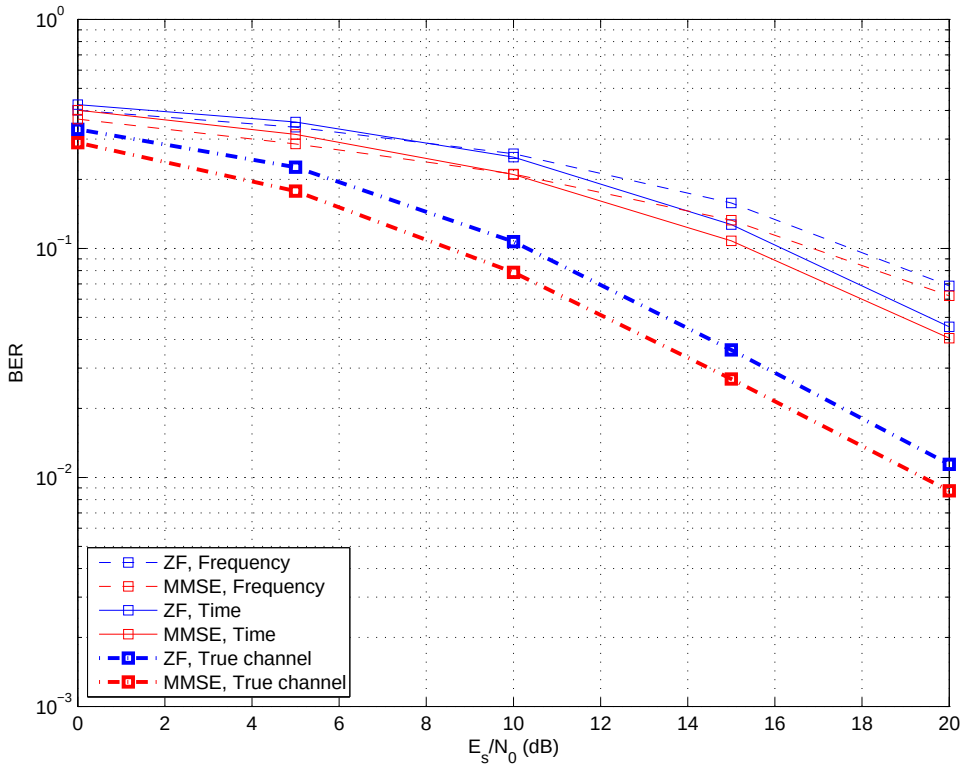

Figure 3.16: Probability of bit error for ZF and MMSE equalizers for 1x2 OFDM with N=64, L=4, M_c=10^4, over 50 uncorrelated channel groups with 16-QAM modulation

From Figure 3.16, one observes that the blind channel estimation results with the MMSE equalizer better than with the ZF equalizer since the ZF equalizer suffers from the noise enhancement on channels. However, in the MMSE equalizer 1/SNR parameter used in the denominator avoids the problems with amplifying the noise. As mentioned in Section 3.3.4, we notice again that the time domain estimation yields smaller BER values than the frequency domain estimation for 16-QAM, which is reversed in the case of QPSK.

3.4 Correlated Channel Characteristics

Finally, we investigate the performance of the time and frequency domain estimation methods with respect to the channel envelope correlation (η). In equation (2.29) the definition of the envelope correlation is given.

In order to observe the effect of envelope correlation between Rayleigh fading channels, correlated Rayleigh fading channels are generated using the correlation matrices ($\boldsymbol{C}_M$) as explained in Section 2.8 with the correlation coefficients (ρ). In these simulations we have assumed

$$\eta_{i,j} = \sqrt{(Re(\rho_{i,j}))^2 + (Im(\rho_{i,j}))^2} \text{ for } 1 \leq i,j \leq M_r \tag{3.7}$$

where $\eta_{i,j}$, $\rho_{i,j}$ are the envelope correlation and correlation coefficient between i^{th} and j^{th} antennas and M_r is the number of receiving antennas. Also we have assumed

$$Re(\rho_{i,j}) = Im(\rho_{i,j}) \text{ for } 1 \leq i,j \leq M_r \tag{3.8}$$

so that channel correlation in the real and imaginary parts are equal to each other.

Figure 2.5 is used to select the appropriate η values for the channel correlations and ρ values are calculated using equations (3.7) and (3.8). η values are chosen using the d/λ values, where d is the distance between antennas and λ is the wavelength. Noting that, chosen η values satisfy the correlation matrix $\boldsymbol{C}_M$ to be positive definite.

Simulations are performed considering equispaced antenna array in the system and some parameters are equal to each other in the correlation matrix as

$$\rho_{i,j} = \rho_{i+k,j+k} \text{ for } 1 \leq i,j \leq M_r \text{ and } 0 \leq k < M_r - i \tag{3.9}$$

Figures 3.17 & 3.18 show the NRMSE and BER comparison of the estimation results of uncorrelated and correlated channels for 1x2 OFDM with N=16, C_p=5, L=4, over 10^4 Monte Carlo runs and 50 channel groups and $\eta_{1,2}$=0, 0.57, 0.71, 0.85, 0.99, where $\eta_{1,2} = \sqrt{(Re(\rho_{1,2}))^2 + (Im(\rho_{1,2}))^2}$ and the correlation matrix is defined as

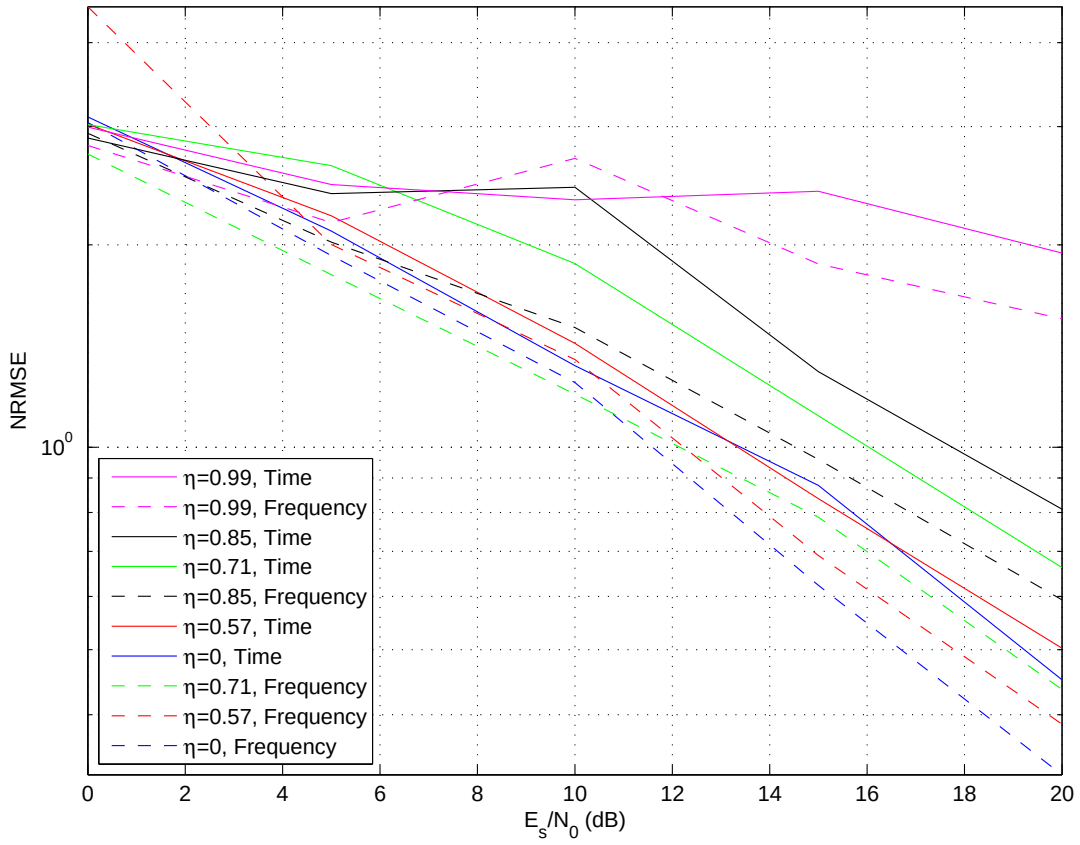

Figure 3.17: Effect of the envelope correlation parameter over NRMSE for 1x2 OFDM, N=16, L=4, M_c=10^4 with QPSK modulation

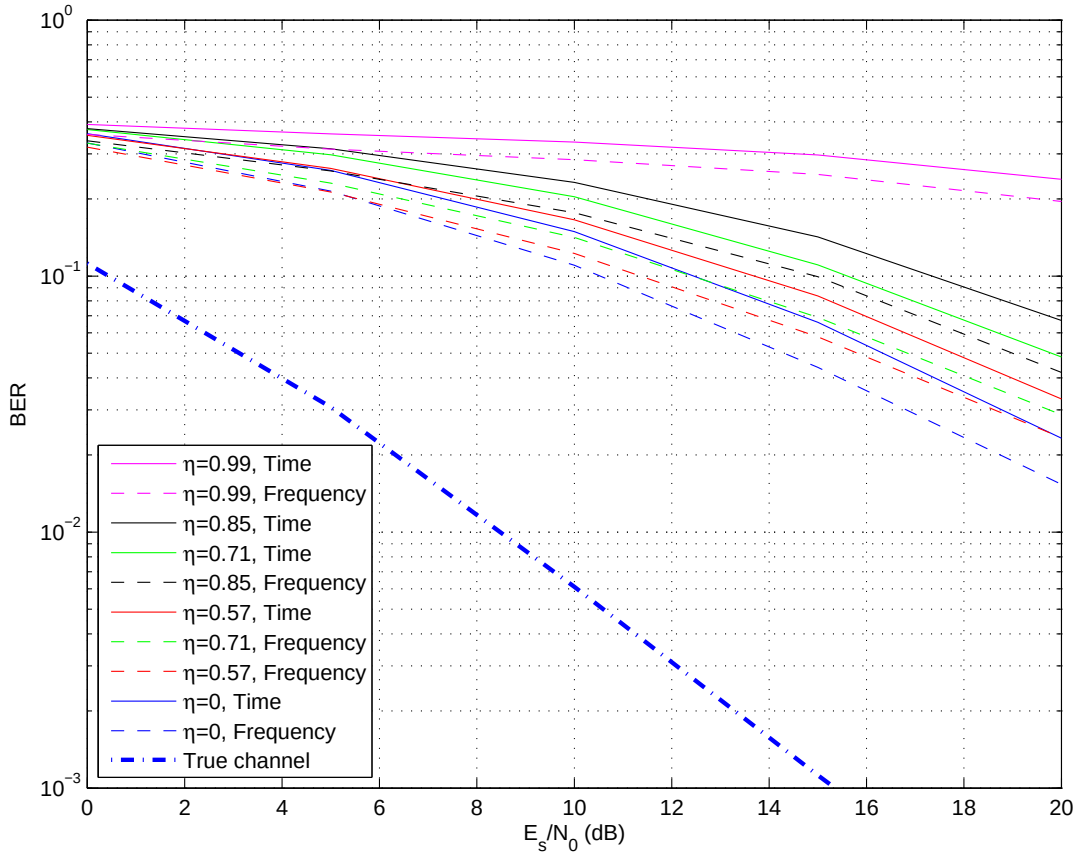

Figure 3.18: Effect of the envelope correlation parameter over probability of bit error for 1x2 OFDM, N=16, L=4, M_c=10^4 with QPSK modulation

$$\boldsymbol{C}_M(\boldsymbol{g}_{1,1}, \boldsymbol{g}_{2,1}) = \begin{bmatrix} 1 & \rho_{1,2} \\ \rho_{1,2}^* & 1 \end{bmatrix}$$

$\rho_{1,2}$ value is determined based on the correlation parameter selection mentioned in Section 2.8. Distances between antennas corresponding to envelope correlations are given in Table 3.3.

As the envelope correlation is increased, Figures 3.17 & 3.18 show that the probability of successful blind channel estimation decreases. Figure 3.18 depicts the effect of increasing the envelope correlation over the bit error rate performances. Both the NRMSE and BER results for the frequency domain estimation method are better than the time domain method as also observed in the other QPSK simulations of this thesis.

Table 3.3: Envelope correlation vs distance for 1x2 OFDM system

Envelope Correlation (η)	$\rho_{1,2}$	Distances (d/λ)
0.99	0.7+0.7j	0.15
0.85	0.6+0.6j	0.45
0.71	0.5+0.5j	0.64
0.57	0.4+0.4j	0.80
0	0+0j	1.45

Figures 3.19 & 3.20 show the NRMSE and BER comparison respectively, of the time and frequency domain blind channel estimation methods with the uncorrelated and correlated channels for 1x3 OFDM with N=16, C_p=5, L=4, over 10^4 Monte Carlo runs and 50 channel groups and envelope correlation parameters ($\eta_{1,2}$, $\eta_{2,3}$)= (0, 0), (0.42, 0.42), (0.57, 0.57) and (0.75, 0.75).

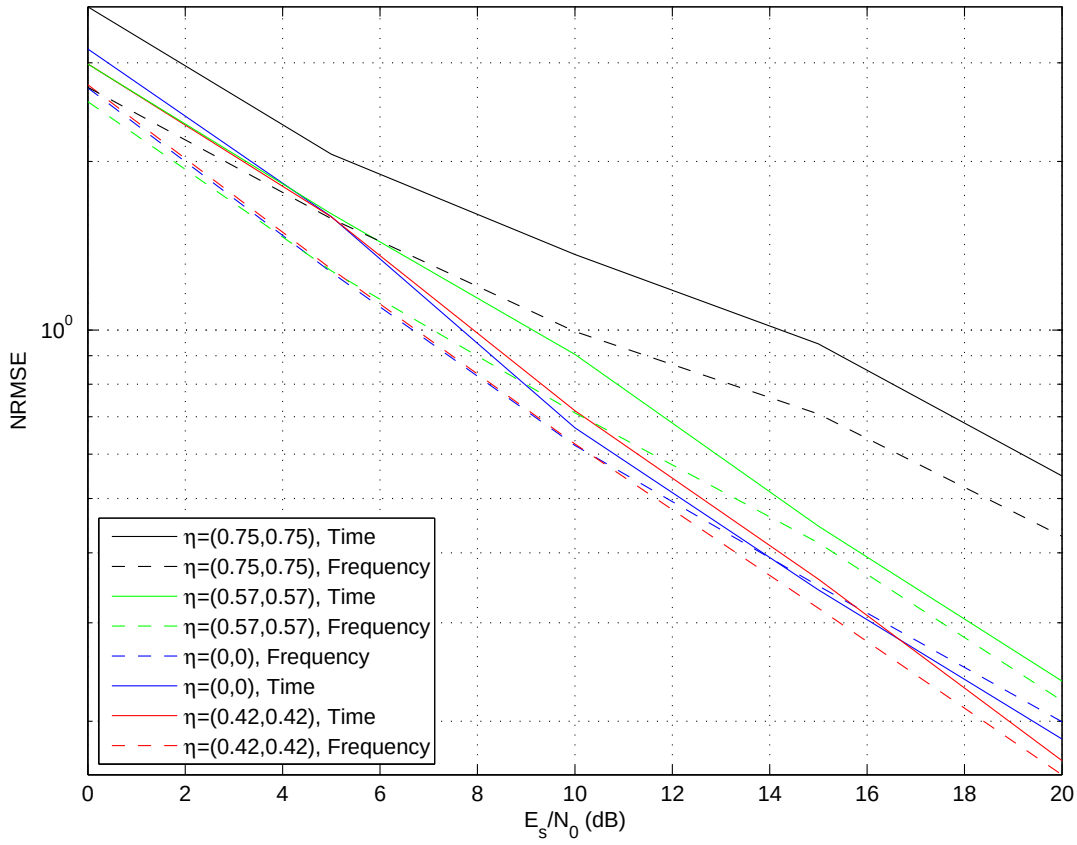

Figure 3.19: Effect of the envelope correlation parameter over NRMSE for 1x3 OFDM, N=16, L=4, M_c=10^4 with QPSK modulation

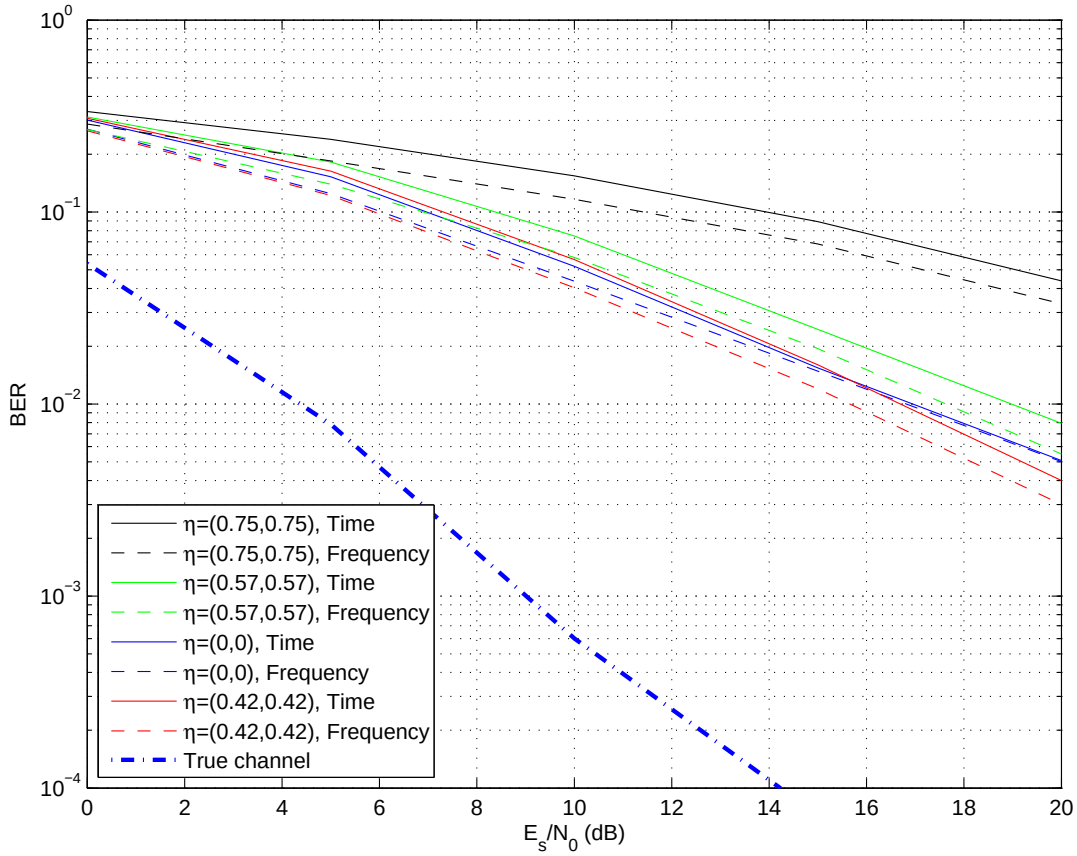

Figure 3.20: Effect of the envelope correlation parameter over probability of bit error for 1x3 OFDM, N=16, L=4, M_c=10^4 with QPSK modulation

The correlation matrix for the 1x3 system is defined as

$$\boldsymbol{C}_M(\boldsymbol{g}_{1,1}, \boldsymbol{g}_{2,1}, \boldsymbol{g}_{3,1}) = \begin{bmatrix} 1 & \rho_{1,2} & \rho_{1,3} \\ \rho_{1,2}^* & 1 & \rho_{2,3} \\ \rho_{1,3}^* & \rho_{2,3}^* & 1 \end{bmatrix}$$

$\rho_{1,2}$, $\rho_{1,3}$ and $\rho_{2,3}$ values are determined based on the correlation parameter selection mentioned in Section 2.8. Distances between antennas corresponding to envelope correlations are given in Table 3.4. Note that, $\rho_{1,2}$ and $\rho_{2,3}$ is equal to each other, since equispaced antenna array is assumed in the system configuration.

As the envelope correlation is increased, successful blind channel estimation rate decreases except for η=0.42. Both in Figures 3.19 & 3.20 results for η=0.42 is better than results of simulation when the uncorrelated channels are used. For η is equal to 0.57 and 0.75, results are worse than the results for the uncorrelated channel case. NRMSE and BER results for the frequency domain method results are better than the time domain method for this simulation.

Table 3.4: Envelope correlation vs distance for 1x3 OFDM system

Envelope Correlations ($\eta_{1,2}$, $\eta_{2,3}$)	$\rho_{1,2}$=$\rho_{2,3}$	$\rho_{1,3}$	Distances (d/λ)
0.75	0.53+0.53j	0.16+0.16j	0.59
0.57	0.4+0.4j	0.07+0.07j	0.80
0.42	0.3+0.3j	0.14+0.14j	0.95
0	0+0j	0+0j	1.45

Figures 3.21 & 3.22 show the NRMSE and BER comparison of respectively, the time and frequency domain blind channel estimation methods with the uncorrelated and correlated channels for 1x4 OFDM with N=16, C_p=5, L=4, over 10^4 Monte Carlo runs and 50 channel groups and envelope correlation parameters
($\rho_{1,2}$, $\rho_{2,3}$, $\rho_{3,4}$) = (0, 0, 0), (0.42, 0.42, 0.42), (0.57, 0.57, 0.57).

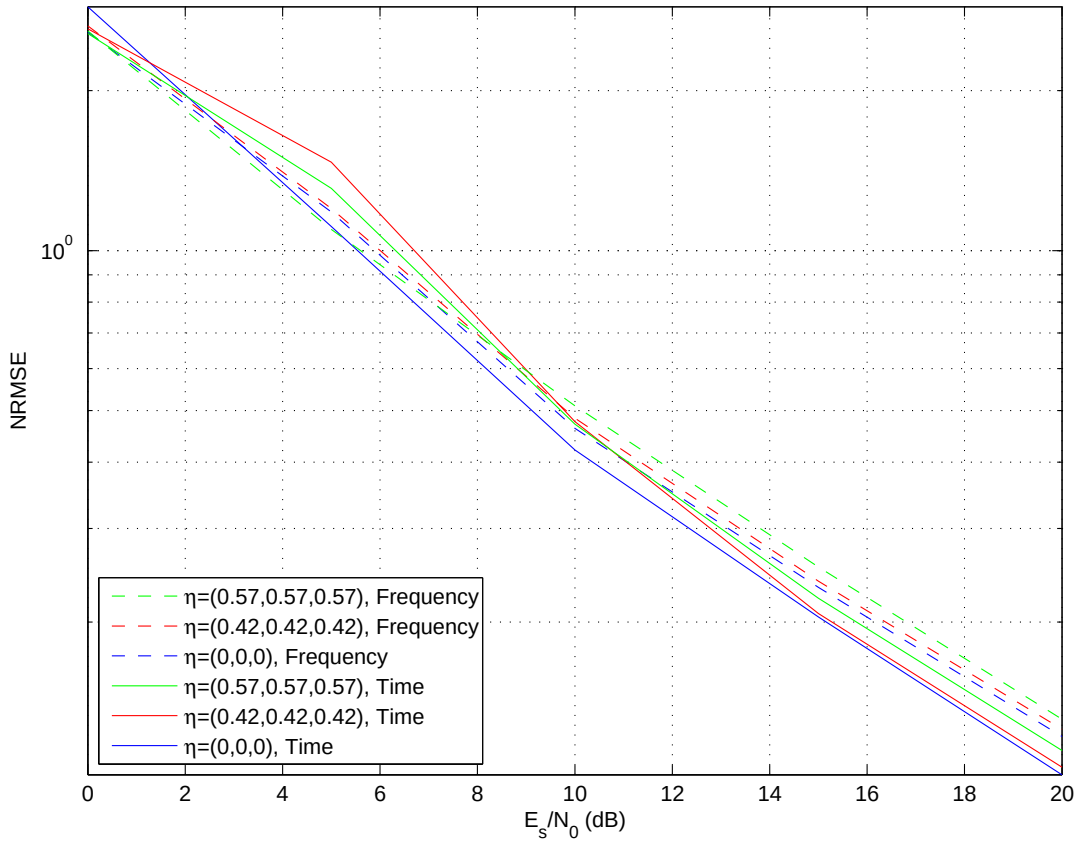

Figure 3.21: Effect of the envelope correlation parameter over NRMSE for 1x4 OFDM, N=16, L=4, M_c=10^4 with QPSK modulation

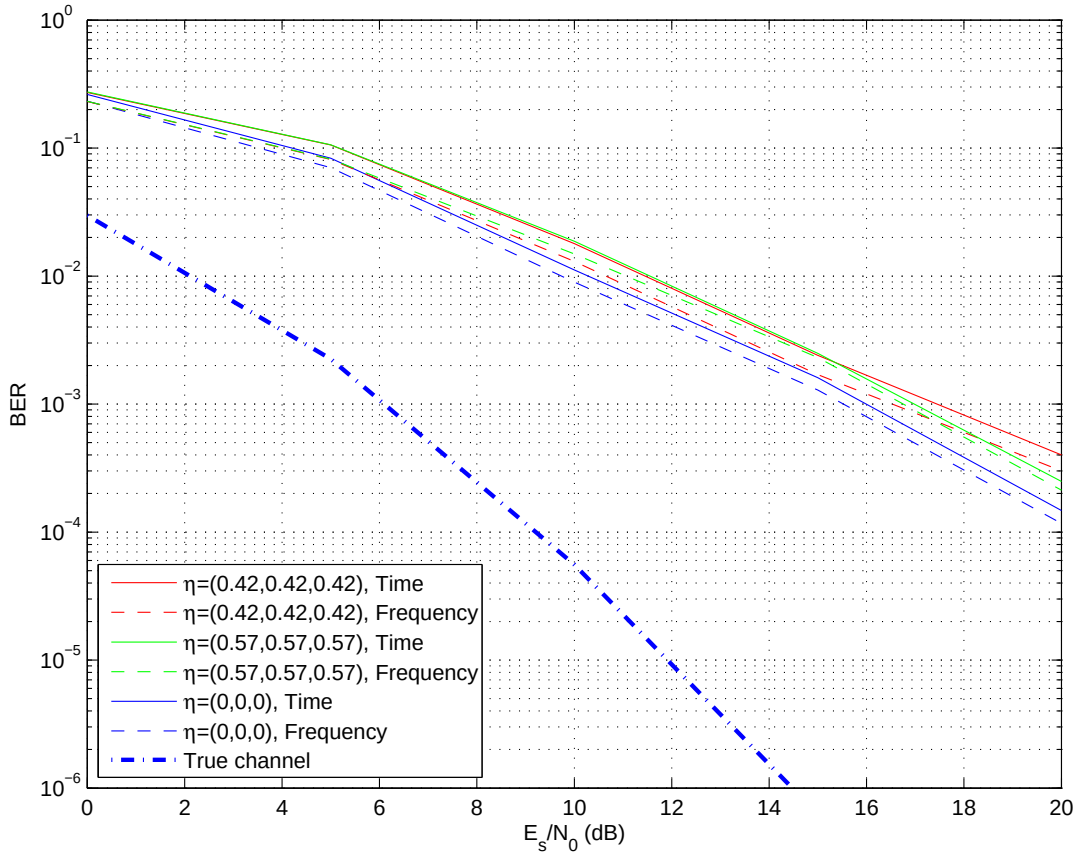

Figure 3.22: Effect of the envelope correlation parameter over probability of bit error for 1x4 OFDM, N=16, L=4, M_c=10^4 with QPSK modulation

The correlation matrix is defined as

$$\boldsymbol{C}_M(\boldsymbol{g}_{1,1},\boldsymbol{g}_{2,1},\boldsymbol{g}_{3,1},\boldsymbol{g}_{4,1}) = \begin{bmatrix} 1 & \rho_{1,2} & \rho_{1,3} & \rho_{1,4} \\ \rho_{1,2}^* & 1 & \rho_{2,3} & \rho_{2,4} \\ \rho_{1,3}^* & \rho_{2,3}^* & 1 & \rho_{3,4} \\ \rho_{1,4}^* & \rho_{2,4}^* & \rho_{3,4}^* & 1 \end{bmatrix}$$

ρ values are determined based on the correlation parameter selection mentioned in Section 2.8. Distances between antennas corresponding to envelope correlations are given in Table 3.5. Again we note that, $\rho_{1,2}$=$\rho_{2,3}$=$\rho_{3,4}$ and $\rho_{1,3}$=$\rho_{2,4}$ since distances between antennas are considered as equal.

As the envelope correlation is increased, all simulations of this section show that the probability of successful blind channel estimation decreases. However, as the number of receiving antennas increase, the sensitivity of the blind estimators versus channel correlation gets smaller; and as observed in Figure 3.22, all BER curves get close to each other and remain between 7.7-9.4 dB SNR loss region with respect to the true

channel performance at BER=10^{-2}. Although such big losses are not at all promising for real world applications, the poor performance of the blind channel estimation methods seems to be overcome by increasing the number of receiving antennas.

Table 3.5: Envelope correlation vs distance for 1x4 OFDM system

Envelope Correlations ($\rho_{1,2}$, $\rho_{2,3}$, $\rho_{3,4}$)	$\rho_{1,2}$=$\rho_{2,3}$=$\rho_{3,4}$	$\rho_{1,3}$=$\rho_{2,4}$	$\rho_{1,4}$	Distances (d/λ)
0.57	0.4+0.4j	0.07+0.07j	0.12+0.12j	0.80
0.42	0.3+0.3j	0.14+0.14j	0.01+0.01j	0.95
0	0+0j	0+0j	0+0j	1.45

CHAPTER 4

CONCLUSION

In this thesis, we have studied cross relation based blind channel estimation methods in SIMO-OFDM systems, namely, the time domain method described by Wang, Lin & Chen [18] and the frequency domain method derived by Park, Chun & Jeong [20]. Simulations have been performed with both the uncorrelated and correlated Rayleigh fading channels using only a single OFDM block at the receiver. Minimum mean squared error equalization, which is replaced by zero forcing equalization in a few trials, is utilized together with the maximum likelihood estimator to estimate the transmitted symbols.

Throughout the simulations, the channel length L and the first time domain gain of the first channel are assumed to be known by the receiver, the latter one being used to resolve the scalar ambiguity. To estimate the channel blindly up to a scalar factor, a two-step estimation, firstly the antenna relation and then the subcarrier relation estimations are used for the frequency domain method, and only one singular value decomposition is utilized for the time domain method. In the noiseless case, both methods perfectly estimate the channels up to a scalar factor.

Performances of these two estimation methods are compared using the mean absolute error (MAE), normalized root mean squared error (NRMSE) and the bit error ratio (BER) curves for different cases. Our QPSK simulations averaged over 50 randomly chosen channel characteristics show that the time domain method generally has smaller MAE. NRMSE curves that we obtain for these two estimation methods are quite close to each other. More specifically, the frequency domain estimator is slightly better for the case of two receiving antennas; and the time domain estima-

tor starts to yield moderately better NRMSE's as the number of receiving antennas increase. If a single channel characteristic is used instead of averaging over 50 channels, this average behavior may be reversed. Such a case is observed in MAE & MSE curves of a specific channel given by Park *et al.* [20], in which the frequency domain estimator has lower MAE & MSE than those of the time domain estimator for SNR's less than 15 dB.

As a comparison of the BER results given by Park *et al.* [20] for QPSK modulation with N=64 subcarriers and a channel of length L=3, we have performed simulations under similar parameters. Although there is no clue in [20] about whether the given curve is for a single channel or it is an average over a random channel ensemble, our results are averaged over 50 randomly produced channels. Table 4.1 presents the required SNR values for a BER=10^{-2}, by time and frequency domain blind channel estimators. In our simulations, we also add the BER curve corresponding to the case of known channel characteristics with no estimators.

Table 4.1: Required SNR for a BER=10^{-2} with QPSK modulation, N=64, L=3

Simulations of	Known Channel	Frequency Domain	Time Domain
Park *et al.* [20],presumably for a single channel, Fig.8		13 dB	18 dB
Ours, averaged over 50 channels, Fig.3.5	9.2 dB	15.5 dB	17.8 dB

It is observed in Table 4.1 that the 5 dB performance gain mentioned in [20] of the frequency domain estimator with respect to the time domain estimator of [18] is as low as 2.3 dB in the 50-channel ensemble that we have produced.

If 16-QAM modulation is used instead of QPSK, we observe that the loss of the time domain estimator relative to the frequency domain method reduces to 1 dB for L=3. Moreover, in our simulations for channel lengths of 4 and 5, the time domain method starts to get slightly better than the frequency domain method for 16-QAM.

To summarize, we can say that whether the blind channel time domain estimator explained by Wang, Lin & Chen [18], or the frequency domain estimator described by Park, Chun & Jeong [20] is used, our simulation results averaged over randomly produced 50 channels do not change substantially. Estimation becomes harder as the channel length increases; hence the performance drops. Similarly, increasing correlation among received channel gains deteriorates the performance of both estimation

methods. On the other hand, with increasing number of receiving antennas, more information is gathered and performances of both estimators improve as expected.

There still remains an important question to be discussed. Table 4.1 indicates an SNR loss of 6.3 dB of the frequency domain estimator, relative to the case of the known channel characteristics. Also, the SNR losses with respect to the known channel performances given in all simulation results of Chapter 3 seem to be excessively high, which may be as large as 12 dB at a BER=10^{-2}, for some cases. Such large SNR losses put reasonable doubt on the practical usage of both blind channel estimation methods. Although one might argue that acceptable BER's could be achieved with more than four receiver antennas, that would also increase the system cost.

In addition to their performance loss, there are drawbacks of the blind estimators considered in this work. Both the channel length and the first gain of the first channel are assumed to be known at the receiver, which are almost impossible to identify in real world conditions. In simulations, we have observed that both estimators are extremely sensitive to estimation errors in the channel length and/or the first channel gain.

Although using only a single OFDM block in the blind channel estimation is well suited for the systems where fast channel variations occur, we think that the performance loss of the blind channel estimators simulated in this work is unacceptably high. It may be the subject of future work to investigate whether it is possible to improve their performance by increasing the number of the OFDM blocks used for estimation without reducing their close channel tracking ability. Even when this is achieved, the problems with the estimation of the channel length and the first channel gain still remain; and in our opinion, the use of training symbols seems to be a more rational choice than the blind channel estimation methods used in this work.

REFERENCES

[1] Wikipedia Encyclopedia, "Wikipedia." http://en.wikipedia.org, last visited on February 2015.

[2] R. W. Chang, "Synthesis of band-limited orthogonal signals for multichannel data transmission," *Bell Systems Tech. Journal*, vol. 45, pp. 1775–1796, December 1966.

[3] B. Saltzberg, "Performance of an Efficient Parallel Data Transmission System," *Communication Technology, IEEE Transactions on*, vol. 15, pp. 805–811, December 1967.

[4] S. Weinstein and P. Ebert, "Data Transmission by Frequency-Division Multiplexing Using the Discrete Fourier Transform," *Communication Technology, IEEE Transactions on*, vol. 19, pp. 628–634, October 1971.

[5] A. Peled and A. Ruiz, "Frequency domain data transmission using reduced computational complexity algorithms," in *Acoustics, Speech, and Signal Processing, IEEE International Conference on ICASSP '80.*, vol. 5, pp. 964–967, Apr 1980.

[6] R. Negi and J. Cioffi, "Pilot tone selection for channel estimation in a mobile OFDM system," *Consumer Electronics, IEEE Transactions on*, vol. 44, pp. 1122–1128, Aug 1998.

[7] M. Morelli and U. Mengali, "A comparison of pilot-aided channel estimation methods for OFDM systems," *Signal Processing, IEEE Transactions on*, vol. 49, pp. 3065–3073, Dec 2001.

[8] F. Wan, W.-P. Zhu, and M. Swamy, "Channel estimation of pulse-shaped multiple-input multiple-output Orthogonal Frequency Division Multiplexing systems," *Communications, IET*, vol. 4, pp. 2104–2114, November 2010.

[9] F. Alayyan, K. Abed-Meraim, and A. Zoubir, "Blind MMSE channel identification and equalization algorithms for OFDM systems," in *Signal Processing and Its Applications, 2007. ISSPA 2007. 9th International Symposium on*, pp. 1–4, Feb 2007.

[10] F. Alayyan, R. Shubair, Y. H. Leung, A. Zoubir, and O. Alketbi, "On MMSE Methods for blind identification of OFDM-based SIMO systems," in *Wireless and Optical Communications Networks, 2009. WOCN '09. IFIP International*

Conference on, pp. 1–5, April 2009.

[11] S. Banani and R. Vaughan, "OFDM With Iterative Blind Channel Estimation," *Vehicular Technology, IEEE Transactions on*, vol. 59, pp. 4298–4308, Nov 2010.

[12] S. Wang and J. Hu, "Blind channel estimation for single-input multiple-output OFDM systems: zero padding based or cyclic prefix based?," *Wireless Communications and Mobile Computing*, vol. 13, no. 2, pp. 204–210, 2013.

[13] N. Miridakis and D. Vergados, "A Survey on the Successive Interference Cancellation Performance for Single-Antenna and Multiple-Antenna OFDM Systems," *Communications Surveys Tutorials, IEEE*, vol. 15, pp. 312–335, First 2013.

[14] X. Li and H. Fan, "Blind channel identification: subspace tracking method without rank estimation," *Signal Processing, IEEE Transactions on*, vol. 49, pp. 2372–2382, Oct 2001.

[15] J. L. Yu, C.-H. Chen, and M.-C. Lee, "Blind Channel Estimation for SIMO OFDM Systems without Cyclic Prefix," in *Wireless Communications, Networking and Mobile Computing, 2006. WiCOM 2006.International Conference on*, pp. 1–4, Sept 2006.

[16] S. Wang and J. Manton, "Blind Channel Estimation for Non-CP OFDM Systems Using Multiple Receive Antennas," *Signal Processing Letters, IEEE*, vol. 16, pp. 299–302, April 2009.

[17] S. Wang and J. Manton, "A Cross-Relation-Based Frequency-Domain Method for Blind SIMO-OFDM Channel Estimation," *Signal Processing Letters, IEEE*, vol. 16, pp. 865–868, Oct 2009.

[18] H. Wang, Y. Lin, and B. Chen, "Data-efficient blind OFDM channel estimation using receiver diversity," *Signal Processing, IEEE Transactions on*, vol. 51, pp. 2613–2623, Oct 2003.

[19] Q. Cheng, H. Wang, and B. Chen, "Joint blind timing synchronization and channel estimation for OFDM using receiver diversity," in *Signals, Systems and Computers, 2002. Conference Record of the Thirty-Sixth Asilomar Conference on*, vol. 1, pp. 649–653 vol.1, Nov 2002.

[20] J.Park, J. Chun, B. J. Jeong, "Cross-relation-based frequency-domain blind channel estimation with multiple antennas in Orthogonal Frequency Division Multiplexing systems," *Communications, IET*, vol. 7, no. 16, pp. 1753 – 1768, 2013.

[21] J. G. Proakis and D. K. Manolakis, *Digital Signal Processing (4th Edition)*.

Upper Saddle River, NJ, USA: Prentice-Hall, Inc., 2006.

[22] J. Salz and J. Winters, "Effect of fading correlation on adaptive arrays in digital mobile radio," *Vehicular Technology, IEEE Transactions on*, vol. 43, pp. 1049–1057, Nov 1994.

[23] A. Yanartaş, *Performance assessment of a BPSK CDMA system using un urban radio channel model*. PhD thesis, Middle East Technical University, 1991.

[24] G. Xu, H. Liu, L. Tong, and T. Kailath, "A least-squares approach to blind channel identification," *Signal Processing, IEEE Transactions on*, vol. 43, pp. 2982–2993, Dec 1995.

[25] H. Cramér, *Mathematical Methods of Statistics*. Princeton University Press, 1946.

[26] C. R. Rao, *Information and the accuracy attainable in the estimation of statistical parameters*. Bulletin of the Calcutta Mathematical Society, 1945.

[27] P. Stoica and B. C. Ng, "On the Cramer-Rao bound under parametric constraints," *Signal Processing Letters, IEEE*, vol. 5, pp. 177–179, July 1998.

[28] K. Inkila, "Homogeneous Least Squares Problem," *The Photogrammetric Journal of Finland*, vol. 19, no. 2, pp. 34–42, 2005.

[29] T. Svoboda, "Least-squares solution of homogeneous equations," 2005.

[30] T. S. Rappaport, *Wireless Communications: Principles and Practice*. Prentice Hall, 2001.

APPENDIX A

MATRICES USED IN CHANNEL ESTIMATIONS

Matrices used for SIMO-OFDM with one-transmitting, two-receiving antennas are given in Sections 2.3.1 and 2.3.2, so these matrices will no longer be mentioned in this appendix.

A.1 Matrices Used in Time Domain Method

In this section, matrices used in the time domain method for SIMO-OFDM with one-transmitting, three-receiving and one-transmitting, four-receiving antennas are given. As mentioned in Section 2.3.1, for the time domain method, we need to minimize the equation (2.10) in order to find channel matrix $\hat{\boldsymbol{g}}$.

For SIMO-OFDM with one-transmitting, three-receiving antennas, cross relation equations for the time domain method can be written for the noiseless case as

$$y_2(n)\boldsymbol{w}_n\boldsymbol{g}_{1,1} - y_1(n)\boldsymbol{w}_n\boldsymbol{g}_{2,1} = 0$$
$$y_3(n)\boldsymbol{w}_n\boldsymbol{g}_{1,1} - y_1(n)\boldsymbol{w}_n\boldsymbol{g}_{3,1} = 0$$
$$y_3(n)\boldsymbol{w}_n\boldsymbol{g}_{2,1} - y_2(n)\boldsymbol{w}_n\boldsymbol{g}_{3,1} = 0$$

where n = 1, ..., N denotes the subcarrier index and the required matrices are given as

$$\hat{\tilde{\boldsymbol{Y}}} = \begin{bmatrix} \tilde{\tilde{\boldsymbol{Y}}}_2\boldsymbol{W}_L & -\tilde{\tilde{\boldsymbol{Y}}}_1\boldsymbol{W}_L & \boldsymbol{0} \\ \tilde{\tilde{\boldsymbol{Y}}}_3\boldsymbol{W}_L & \boldsymbol{0} & -\tilde{\tilde{\boldsymbol{Y}}}_1\boldsymbol{W}_L \\ \boldsymbol{0} & \tilde{\tilde{\boldsymbol{Y}}}_3\boldsymbol{W}_L & -\tilde{\tilde{\boldsymbol{Y}}}_2\boldsymbol{W}_L \end{bmatrix} \in \mathbb{C}^{3N\times 3L} \quad \hat{\boldsymbol{g}} = \begin{bmatrix} \hat{\boldsymbol{g}}_{1,1} \\ \hat{\boldsymbol{g}}_{2,1} \\ \hat{\boldsymbol{g}}_{3,1} \end{bmatrix} \in \mathbb{C}^{3L\times 1}$$

For SIMO-OFDM with one-transmitting, four-receiving antennas, there are three more equations compared to the SIMO-OFDM with one-transmitting, three-receiving antennas in the cross relation functions for the time domain method in the noiseless case. These equations are given as

$$
\begin{aligned}
y_2(n)\boldsymbol{w}_n\boldsymbol{g}_{1,1} - y_1(n)\boldsymbol{w}_n\boldsymbol{g}_{2,1} &= 0 \\
y_3(n)\boldsymbol{w}_n\boldsymbol{g}_{1,1} - y_1(n)\boldsymbol{w}_n\boldsymbol{g}_{3,1} &= 0 \\
y_4(n)\boldsymbol{w}_n\boldsymbol{g}_{1,1} - y_1(n)\boldsymbol{w}_n\boldsymbol{g}_{4,1} &= 0 \\
y_3(n)\boldsymbol{w}_n\boldsymbol{g}_{2,1} - y_2(n)\boldsymbol{w}_n\boldsymbol{g}_{3,1} &= 0 \\
y_4(n)\boldsymbol{w}_n\boldsymbol{g}_{2,1} - y_2(n)\boldsymbol{w}_n\boldsymbol{g}_{4,1} &= 0 \\
y_4(n)\boldsymbol{w}_n\boldsymbol{g}_{3,1} - y_3(n)\boldsymbol{w}_n\boldsymbol{g}_{4,1} &= 0
\end{aligned}
$$

and the required matrices become

$$
\hat{\bar{\boldsymbol{Y}}} = \begin{bmatrix}
\tilde{\bar{\boldsymbol{Y}}}_2\boldsymbol{W}_L & -\tilde{\bar{\boldsymbol{Y}}}_1\boldsymbol{W}_L & \boldsymbol{0} & \boldsymbol{0} \\
\tilde{\bar{\boldsymbol{Y}}}_3\boldsymbol{W}_L & \boldsymbol{0} & -\tilde{\bar{\boldsymbol{Y}}}_1\boldsymbol{W}_L & \boldsymbol{0} \\
\tilde{\bar{\boldsymbol{Y}}}_4\boldsymbol{W}_L & \boldsymbol{0} & \boldsymbol{0} & -\tilde{\bar{\boldsymbol{Y}}}_1\boldsymbol{W}_L \\
\boldsymbol{0} & \tilde{\bar{\boldsymbol{Y}}}_3\boldsymbol{W}_L & -\tilde{\bar{\boldsymbol{Y}}}_2\boldsymbol{W}_L & \boldsymbol{0} \\
\boldsymbol{0} & \tilde{\bar{\boldsymbol{Y}}}_4\boldsymbol{W}_L & \boldsymbol{0} & -\tilde{\bar{\boldsymbol{Y}}}_2\boldsymbol{W}_L \\
\boldsymbol{0} & \boldsymbol{0} & \tilde{\bar{\boldsymbol{Y}}}_4\boldsymbol{W}_L & -\tilde{\bar{\boldsymbol{Y}}}_3\boldsymbol{W}_L
\end{bmatrix} \in \mathbb{C}^{4N\times 4L} \qquad \hat{\boldsymbol{g}} = \begin{bmatrix}
\hat{\boldsymbol{g}}_{1,1} \\ \hat{\boldsymbol{g}}_{2,1} \\ \hat{\boldsymbol{g}}_{3,1} \\ \hat{\boldsymbol{g}}_{4,1}
\end{bmatrix} \in \mathbb{C}^{4L\times 1}
$$

Using $\hat{\bar{\boldsymbol{Y}}}$ matrix in the Singular Value Decomposition, we estimate the channel matrix $\hat{\boldsymbol{g}}$ up to a scalar ambiguity factor.

A.2 Matrices Used in Frequency Domain Method

In this section, matrices used in the frequency domain method for SIMO-OFDM with one-transmitting, three-receiving and one-transmitting, four-receiving antennas are given. For the frequency domain method, we need to minimize the equation (2.15) for each subcarriers as described in section 2.3.2 in order to find $\hat{\boldsymbol{h}}^s(n)$ matrices for n=1, ..., N where n denotes the subcarrier index.

For SIMO-OFDM with one-transmitting, three-receiving antennas, cross relation equations for the frequency domain method are defined for the noiseless case as

$$
\begin{aligned}
y_2(n)h^s_{1,1}(n) - y_1(n)h^s_{2,1}(n) &= 0 \\
y_3(n)h^s_{1,1}(n) - y_1(n)h^s_{3,1}(n) &= 0 \\
y_3(n)h^s_{2,1}(n) - y_2(n)h^s_{3,1}(n) &= 0
\end{aligned}
$$

and the required matrices are given as

$$
\hat{\boldsymbol{Y}}(n) = \begin{bmatrix} \hat{y}_2(n) & -\hat{y}_1(n) & 0 \\ \hat{y}_3(n) & 0 & -\hat{y}_1(n) \\ 0 & \hat{y}_3(n) & -\hat{y}_2(n) \end{bmatrix} \in \mathbb{C}^{3\times 3} \qquad \hat{\boldsymbol{h}}^s(n) = \begin{bmatrix} \hat{h}^s_{1,1}(n) \\ \hat{h}^s_{2,1}(n) \\ \hat{h}^s_{3,1}(n) \end{bmatrix} \in \mathbb{C}^{3\times 1}
$$

For SIMO-OFDM with one-transmitting, four-receiving antennas, there are six cross relation functions for the frequency domain method for the noiseless case. These equations are given as

$$
\begin{aligned}
y_2(n)h^s_{1,1}(n) - y_1(n)h^s_{2,1}(n) &= 0 \\
y_3(n)h^s_{1,1}(n) - y_1(n)h^s_{3,1}(n) &= 0 \\
y_4(n)h^s_{1,1}(n) - y_1(n)h^s_{4,1}(n) &= 0 \\
y_3(n)h^s_{2,1}(n) - y_2(n)h^s_{3,1}(n) &= 0 \\
y_4(n)h^s_{2,1}(n) - y_2(n)h^s_{4,1}(n) &= 0 \\
y_4(n)h^s_{3,1}(n) - y_3(n)h^s_{4,1}(n) &= 0
\end{aligned}
$$

and the required matrices are given as

$$\hat{\boldsymbol{Y}}(n) = \begin{bmatrix} \hat{y}_2(n) & -\hat{y}_1(n) & 0 & 0 \\ \hat{y}_3(n) & 0 & -\hat{y}_1(n) & 0 \\ \hat{y}_4(n) & 0 & 0 & -\hat{y}_1(n) \\ 0 & \hat{y}_3(n) & -\hat{y}_2(n) & 0 \\ 0 & \hat{y}_4(n) & 0 & -\hat{y}_2(n) \\ 0 & 0 & \hat{y}_4(n) & -\hat{y}_3(n) \end{bmatrix} \in \mathbb{C}^{4\times 4} \quad \hat{\boldsymbol{h}}^{s}(n) = \begin{bmatrix} \hat{h}^{s}_{1,1}(n) \\ \hat{h}^{s}_{2,1}(n) \\ \hat{h}^{s}_{3,1}(n) \\ \hat{h}^{s}_{4,1}(n) \end{bmatrix} \in \mathbb{C}^{4\times 1}$$

Using $\hat{\boldsymbol{Y}}(n)$ matrices in the Eigen Value Decomposition, we estimate the $\hat{\boldsymbol{h}}^{s}(n)$ matrices for the Antenna Relation Estimation for each subcarrier as mentioned in section 2.3.2.

APPENDIX B

SOLUTION OF HOMOGENEOUS LEAST SQUARES PROBLEM

In this section solution of equation (2.16) is given. For the solution of the Homogeneous Least Squares problem, Lagrange multipliers derivation is explained for transpose of a matrix instead of conjugate transpose matrix.

Solution that minimizes $\boldsymbol{h}^T\hat{\boldsymbol{Y}}^T\hat{\boldsymbol{Y}}\boldsymbol{h}$ with constrain $\|\boldsymbol{h}\| = 1$ can be found using *Lagrange Method* with minimizing

$$L(\boldsymbol{h}, \lambda) = \boldsymbol{h}^T\boldsymbol{Y}^T\boldsymbol{Y}\boldsymbol{h} + \lambda(1 - \boldsymbol{h}^T\boldsymbol{h}) \tag{B.1}$$

where λ is the Lagrange multiplier. Taking partial derivatives of L with respect to λ and $\boldsymbol{h}$ and setting these equations to zero, we obtain

$$\boldsymbol{Y}^T\boldsymbol{Y}\boldsymbol{h} = \lambda\boldsymbol{h} \tag{B.2}$$

and

$$\boldsymbol{h}^T\boldsymbol{h} = 1 \tag{B.3}$$

Using equation (B.1) we get

$$L = \boldsymbol{h}^T\boldsymbol{Y}^T\boldsymbol{Y}\boldsymbol{h} + \lambda(1 - \boldsymbol{h}^T\boldsymbol{h}) = \boldsymbol{h}^T(\boldsymbol{Y}^T\boldsymbol{Y}\boldsymbol{h} - \lambda\boldsymbol{h}) + \lambda = \lambda \tag{B.4}$$

Thus, the Least Squares solution is the eigenvector corresponding to the smallest eigenvalue of $\boldsymbol{Y}^T\boldsymbol{Y}$ [28, 29].

APPENDIX C

NRMSE VERSUS MSE

Figure C.1 shows the MSE and NRMSE comparison of the estimation results of uncorrelated channels for 1x2 OFDM with N=64, L=3, over 10^4 Monte Carlo runs and 50 channel groups. In Figures C.2 & C.3 MSE and NRMSE results are compared for L=4 and 5 respectively.

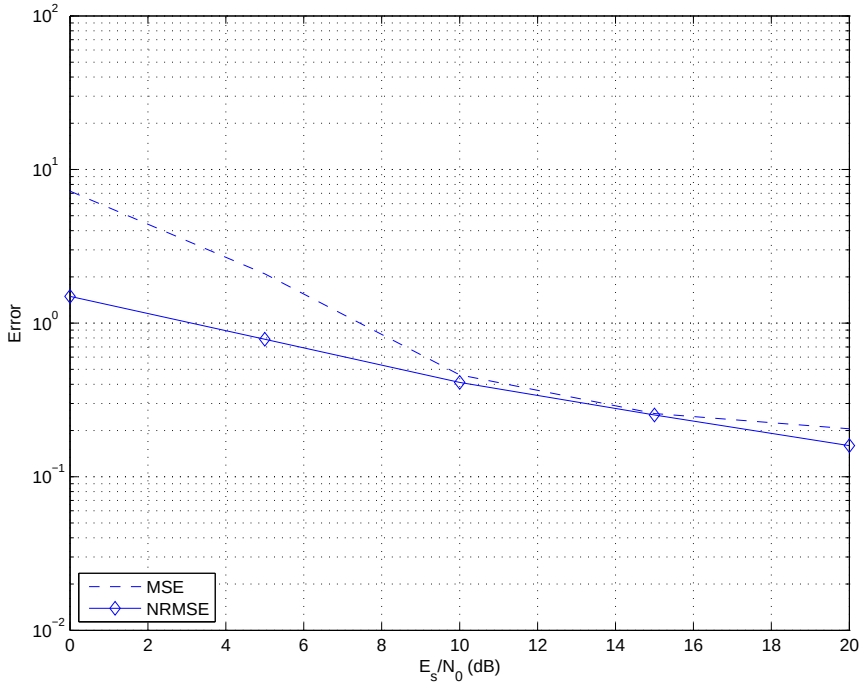

Figure C.1: SNR versus MSE and NRMSE for M_r=2, N=64, L=3, M_c=10^4, over 50 uncorrelated channel groups with QPSK modulation

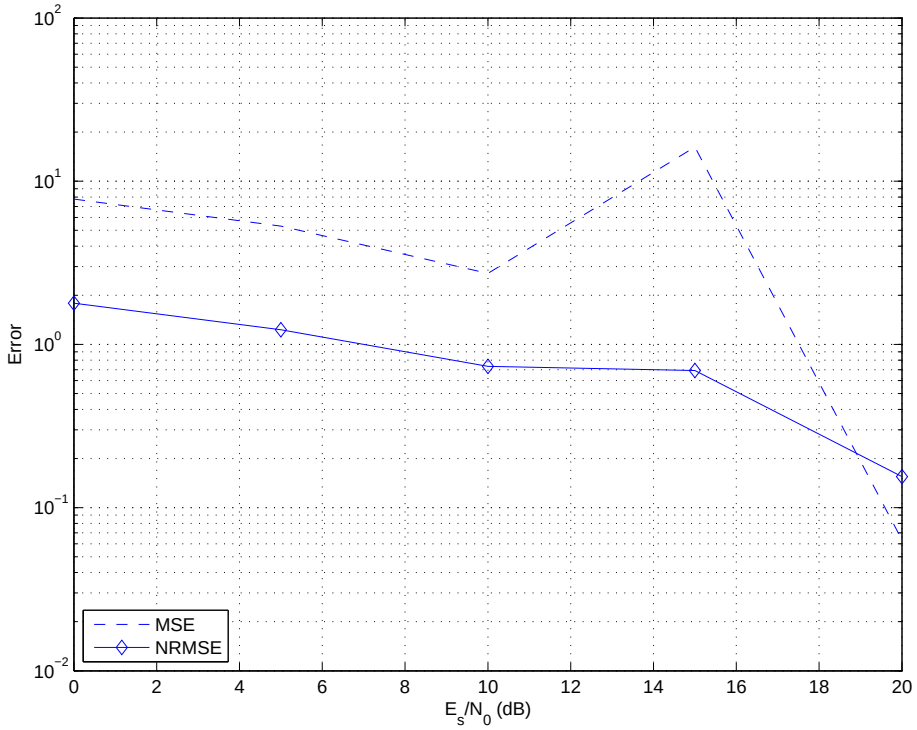

Figure C.2: SNR versus MSE and NRMSE for M_r=2, N=64, L=4, M_c=10^4, over 50 uncorrelated channel groups with QPSK modulation

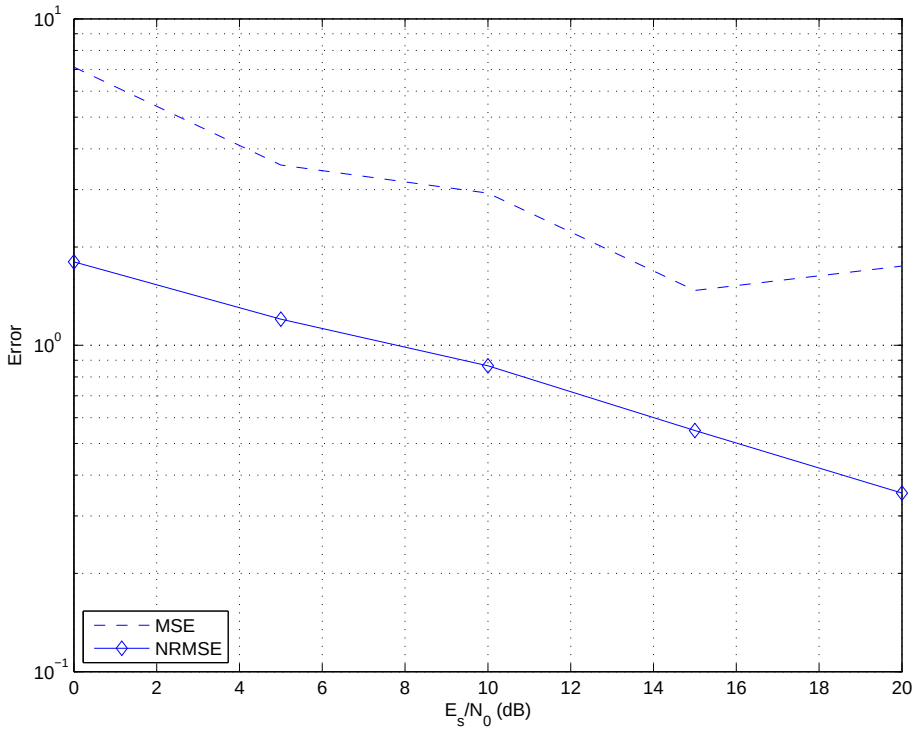

Figure C.3: SNR versus MSE and NRMSE for M_r=2, N=64, L=5, M_c=10^4, over 50 uncorrelated channel groups with QPSK modulation

It is inferred from Figures C.1, C.2 & C.3 that, the square rooting operation of the NRMSE defined by equations (3.3) & (3.6) as in [24] makes a smoothing effect on the MSE and reduces the effect of unreasonably high terms. For that reason, we prefer the NRMSE measure over MSE as a more reliable performance criterion.

APPENDIX D

CALCULATION OF CRAMER RAO BOUND

In the Cramer Rao Bound calculation, derivation in [18] is modified by replacing **d**, **D** and $\mathbf{W}_{L+1}$ matrices with $\boldsymbol{s}$, $\boldsymbol{S}$ and $\boldsymbol{W}_L$ respectively. Considering the signal model as in (2.4), the unknown vector can be defined as

$$\boldsymbol{\theta} = [Re(\boldsymbol{g}_1), Re(\boldsymbol{g}_2), Re(\boldsymbol{s}), Im(\boldsymbol{g}_1), Im(\boldsymbol{g}_2), Im(\boldsymbol{s})]$$

We define $\boldsymbol{\mu}$ matrix as

$$\boldsymbol{\mu} = \begin{bmatrix} \boldsymbol{s}\mathrm{W}_L\boldsymbol{g}_1 \\ \boldsymbol{s}\mathrm{W}_L\boldsymbol{g}_2 \end{bmatrix}$$

to be the mean value of the observation vector $[\mathbf{y}_1, \mathbf{y}_2]^T$ that is otherwise Gaussian distributed. Each element of the the Fisher Information Matrix FIM, denoted by $\boldsymbol{F}$ can be written, given that noise covariance matrix $\sigma^2\mathbf{I}$, as

$$\boldsymbol{F}(i,j) = \frac{2}{\sigma^2} Re\left[(\frac{\partial \boldsymbol{\mu}}{\partial \theta_i})^H \ \ \frac{\partial \boldsymbol{\mu}}{\partial \theta_j}) \right]$$

Define $\tilde{\boldsymbol{\theta}} = [\boldsymbol{g}_1, \boldsymbol{g}_2, \boldsymbol{s}]$. In matrix form, $\boldsymbol{F}$ can be written as [18]

$$\boldsymbol{F} = 2 \begin{bmatrix} Re(\boldsymbol{F}_c) & -Im(\boldsymbol{F}_c) \\ Im(\boldsymbol{F}_c) & Re(\boldsymbol{F}_c) \end{bmatrix}$$

where each element of $\boldsymbol{F}_c$ is

$$\boldsymbol{F}_c(i,j) = \frac{2}{\sigma^2} Re\left[(\frac{\partial \boldsymbol{\mu}}{\partial \tilde{\theta}_i})^H \ \ \frac{\partial \boldsymbol{\mu}}{\partial \tilde{\theta}_j}) \right]$$

Write $\boldsymbol{F}_c$ in partitioned matrix form as

$$\boldsymbol{F}_c = \frac{1}{\sigma^2} \begin{bmatrix} \boldsymbol{A}_{11} & \boldsymbol{A}_{12} & \boldsymbol{A}_{13} \\ \boldsymbol{A}_{21} & \boldsymbol{A}_{22} & \boldsymbol{A}_{23} \\ \boldsymbol{A}_{31} & \boldsymbol{A}_{32} & \boldsymbol{A}_{33} \end{bmatrix}$$

Defining $\boldsymbol{Q} = \boldsymbol{S}\boldsymbol{W}_L$, where $\boldsymbol{S}$ is a diagonal matrix with entries $\boldsymbol{s}_{mt}$ we can calculate each parameter matrix of $\boldsymbol{F}_c$ as:

$$\boldsymbol{A}_{11} = \frac{\partial \boldsymbol{\mu}^H}{\partial \boldsymbol{g}_1}\frac{\partial \boldsymbol{\mu}}{\partial \boldsymbol{g}_1^H} = [\boldsymbol{W}_L\boldsymbol{S}^H \;\; 0][\boldsymbol{S}\boldsymbol{W}_L \;\; 0]^T = \boldsymbol{Q}^H\boldsymbol{Q}$$

$$\boldsymbol{A}_{12} = \frac{\partial \boldsymbol{\mu}^H}{\partial \boldsymbol{g}_1}\frac{\partial \boldsymbol{\mu}}{\partial \boldsymbol{g}_2^H} = [\boldsymbol{W}_L\boldsymbol{S}^H \;\; 0][0 \;\; \boldsymbol{S}\boldsymbol{W}_L]^T = \boldsymbol{0}$$

$$\boldsymbol{A}_{13} = \frac{\partial \boldsymbol{\mu}^H}{\partial \boldsymbol{g}_1}\frac{\partial \boldsymbol{\mu}}{\partial \boldsymbol{s}^H} = [\boldsymbol{W}_L\boldsymbol{S}^H \;\; 0][\boldsymbol{H}_1 \;\; 0]^T = \boldsymbol{Q}^H\boldsymbol{H}_1$$

$$\boldsymbol{A}_{21} = \frac{\partial \boldsymbol{\mu}^H}{\partial \boldsymbol{g}_2}\frac{\partial \boldsymbol{\mu}}{\partial \boldsymbol{g}_1^H} = [0 \;\; \boldsymbol{W}_L\boldsymbol{S}^H][\boldsymbol{S}\boldsymbol{W}_L \;\; 0]^T = \boldsymbol{0}$$

$$\boldsymbol{A}_{22} = \frac{\partial \boldsymbol{\mu}^H}{\partial \boldsymbol{g}_2}\frac{\partial \boldsymbol{\mu}}{\partial \boldsymbol{g}_2^H} = [0 \;\; \boldsymbol{W}_L\boldsymbol{S}^H][0 \;\; \boldsymbol{S}\boldsymbol{W}_L]^T = \boldsymbol{Q}^H\boldsymbol{Q}$$

$$\boldsymbol{A}_{23} = \frac{\partial \boldsymbol{\mu}^H}{\partial \boldsymbol{g}_2}\frac{\partial \boldsymbol{\mu}}{\partial \boldsymbol{s}^H} = [0 \;\; \boldsymbol{W}_L\boldsymbol{S}^H][0 \;\; \boldsymbol{H}_2]^T = \boldsymbol{Q}^H\boldsymbol{H}_2$$

$$\boldsymbol{A}_{31} = \frac{\partial \boldsymbol{\mu}^H}{\partial \boldsymbol{s}}\frac{\partial \boldsymbol{\mu}}{\partial \boldsymbol{g}_1^H} = [\boldsymbol{H}_1^H \;\; \boldsymbol{H}_2^H][\boldsymbol{S}\boldsymbol{W}_L \;\; 0]^T = \boldsymbol{H}_1^H\boldsymbol{Q}$$

$$\boldsymbol{A}_{32} = \frac{\partial \boldsymbol{\mu}^H}{\partial \boldsymbol{s}}\frac{\partial \boldsymbol{\mu}}{\partial \boldsymbol{g}_2^H} = [\boldsymbol{H}_1^H \;\; \boldsymbol{H}_2^H][0 \;\; \boldsymbol{S}\boldsymbol{W}_L]^T = \boldsymbol{H}_2^H\boldsymbol{Q}$$

$$\boldsymbol{A}_{33} = \frac{\partial \boldsymbol{\mu}^H}{\partial \boldsymbol{s}}\frac{\partial \boldsymbol{\mu}}{\partial \boldsymbol{s}^H} = [\boldsymbol{H}_1^H \;\; \boldsymbol{H}_2^H][\boldsymbol{H}_1 \;\; \boldsymbol{H}_2]^T = \boldsymbol{H}_1^H\boldsymbol{H}_1 + \boldsymbol{H}_2^H\boldsymbol{H}_2$$

Finally,

$$\boldsymbol{F}_c = \frac{1}{\sigma^2}\begin{bmatrix} \boldsymbol{Q}^H\boldsymbol{Q} & \boldsymbol{0} & \boldsymbol{Q}^H\boldsymbol{H}_1 \\ \boldsymbol{0} & \boldsymbol{Q}^H\boldsymbol{Q} & \boldsymbol{Q}^H\boldsymbol{H}_2 \\ \boldsymbol{H}_1\boldsymbol{Q} & \boldsymbol{H}_2^H\boldsymbol{Q} & \boldsymbol{H}_1^H\boldsymbol{H}_1 + \boldsymbol{H}_2^H\boldsymbol{H}_2 \end{bmatrix}$$

APPENDIX E

SMALL SCALE FADING

E.1 Small Scale Fading

Fading occurs when multiple copies of the transmitted signal arrive at the receiver antenna with different time delays. The copies of the transmitted signal, called multipath signals, form a resultant signal which can vary extensively in amplitude and phase depending on the environment of the transmitter and receiver, time delay and the bandwidth of the transmitted signal.

In this appendix we will discuss the multipath propagation, factors of fading, present mathematical model and time and frequency characterization of fading.

E.1.1 Small Scale Multipath Propagation

In urban area, fading occurs because there is no line-of-sight (LOS) path between mobile station and base station. Even if LOS exists, fading still occurs because of the reflection from ground surface and surrounding structures like buildings, cars etc. The received signal at mobile station consists of multiple copies of the transmitted signal that come from different directions and time delays. Each multipath signal has a randomly distributed amplitude, phase and direction of arrival. These multipath signals combine vectorially at the receiver and cause fading or distortion on the received signal. Even if a mobile receiver is stationary, the received signal may fade because of the movement of the surrounding objects like human beings, cars etc in the channel.

Due to the relative motion between the mobile and the base station, each multipath

wave experiences an apparent shift in frequency. The shift in received signal frequency due to the motion is called the Doppler shift, and is directly proportional to the velocity and direction of motion of the mobile with respect to the direction of arrival of the received multipath wave. Multipath propagation scenario is shown in Figure E.1.

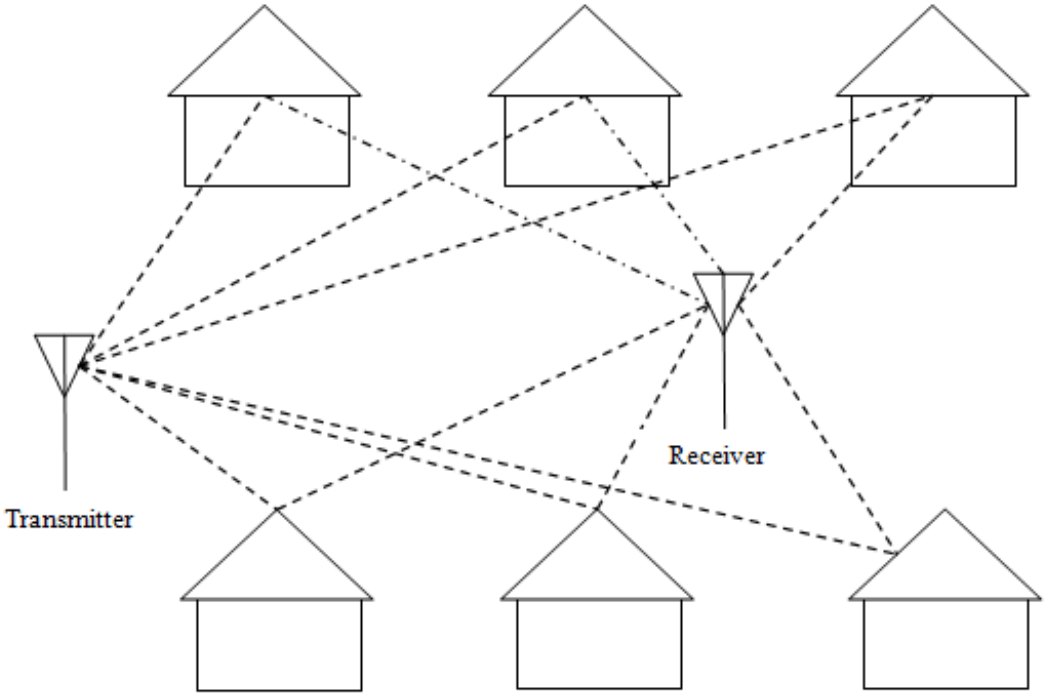

Figure E.1: Multipath propagation

E.1.2 Doppler Shift

Consider a mobile station moving from point A to point B at a constant velocity v while it is receiving signal from source S as shown in Figure E.2. The difference in path lengths traveled by signal wave is $\Delta l = |AS| - |BS| = d\cos\alpha = v\Delta t\cos\alpha$, where Δt is the time required for the mobile station to reach to the point B from point A. α angles are assumed to be the same, considering the source S is much far away from the mobile station. The change in phase of the received signal due to Δl is then represented as

$$\Delta\phi = \frac{2\pi\Delta l}{\lambda} = \frac{2\pi v\Delta t\cos\alpha}{\lambda} \tag{E.1}$$

and the change in frequency (Doppler Shift) is represented by f_d, where

$$f_d = \frac{1}{2\pi}\frac{\Delta\phi}{\Delta t} = \frac{v\cos\alpha}{\lambda} \tag{E.2}$$

where λ is the wavelength of the received signal.

Equation (E.2) shows the relation between the Doppler shift and velocity, wavelength and arrival angle of the wave. f_d is positive if the mobile station is moving towards the direction of arrival of the wave, meaning increase in received frequency. Otherwise, f_d is negative, meaning decrease in received frequency.

Multipath components from a continuous wave signal that arrive from different directions contribute to Doppler spreading of the received signal, thus increasing the signal bandwidth [30].

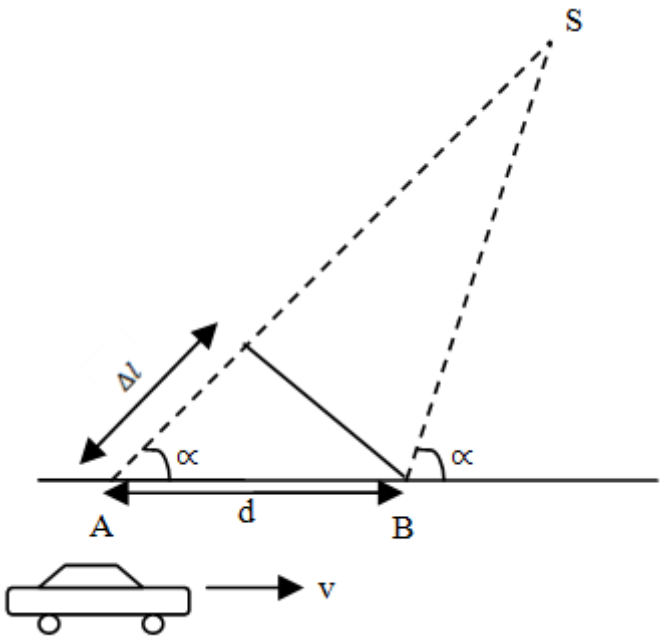

Figure E.2: Illustration of Doppler effect [30]

E.1.3 Mathematical Model of Fading

In this section mathematical model of fading is derived.

Let us consider a bandpass signal $x(t)$ is transmitted with a complex envelope $\overline{x}(t)$ at

a carrier frequency f_c. The transmitted signal $x(t)$ can be written as

$$x(t) = \mathbf{Re}\Big\{\overline{x}(t)e^{j2\pi f_c t}\Big\} \tag{E.3}$$

and the received signal $y(t)$ can be written as

$$y(t) = \mathbf{Re}\Big\{\overline{y}(t)e^{j2\pi f_c t}\Big\} \tag{E.4}$$

where $\overline{y}(t)$ is the complex envelope of the $y(t)$.

As we described in section E.1.1, the received signal consists of multiple copies of the transmitted signal having different attenuations and time delays. Assuming there is no motion in the environment of the base station and mobile station, the resultant signal $y(t)$ can be written as a combination of these multipath signals as

$$y(t) = \sum_i \alpha_i x(t - \frac{l_i}{c}) = \mathbf{Re}\Bigg\{\sum_i \alpha_i \overline{x}(t - \frac{l_i}{c})e^{2\pi f_c(t - \frac{l_i}{c})}\Bigg\} \tag{E.5}$$

where l_i is the path difference of the i^{th} multipath and c is the speed of light. $\overline{y}(t)$, the complex envelope of $y(t)$ can be written as

$$\overline{y}(t) = \sum_i \alpha_i \overline{x}(t - \frac{l_i}{c})e^{-2\pi f_c \frac{l_i}{c}} \tag{E.6}$$

Defining $\tau_i = \frac{l_i}{c}$, above equation becomes

$$\overline{y}(t) = \sum_i \alpha_i \overline{x}(t - \tau_i)e^{-2\pi f_c \tau_i} \tag{E.7}$$

In the case of movement of environment, we need to include the effect of the Doppler shift and the equation (E.7) becomes

$$\overline{y}(t) = \sum_i \alpha_i \overline{x}(t - \tau_i)e^{-2\pi (f_c + \Delta f_i)\tau_i} \tag{E.8}$$

where Δf_i is the Doppler shift in the frequency that belongs to the i^{th} multipath signal. Thus, using equation (E.4) and equation (E.8) the received signal $y(t)$ can be written as

$$y(t) = \mathbf{Re}\Bigg\{\sum_i \alpha_i \overline{x}(t - \tau_i)e^{2\pi (f_c + \Delta f_i)(t - \tau_i)}\Bigg\} \tag{E.9}$$

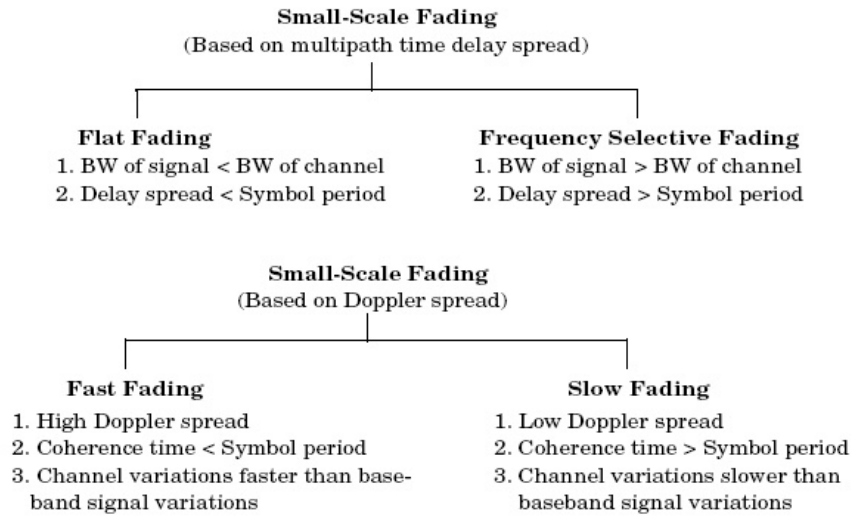

Figure E.3: Types of small-scale fading [30]

E.1.4 Types of Small Scale Fading

Types of small-scale fading can be separated into two parts based on the multipath time delay spread and the Doppler spread. Depending on the relation between the signal parameters (such as bandwidth, symbol period, etc.) and the channel parameters (such as rms delay spread and Doppler spread), different transmitted signals will undergo different types of fading [30]. Four different types of small-scale fading is shown in Figure E.3.

E.1.4.1 Flat Fading

A mobile radio channel is called flat fading if

$$B_S \ll B_C \tag{E.10}$$

and

$$T_S \gg \sigma_\tau \tag{E.11}$$

where B_S, B_C, T_S and σ_τ denotes bandwidth of transmitted signal, coherence bandwidth, sampling time and rms delay spread respectively. In flat fading, each frequency component of the transmitted signal come across with the same magnitude of fading and the spectral characteristics of the transmitted signal is not distorted through the

channel. Flat fading channels are also called as narrowband channels, since the bandwidth of the transmitted signal is narrower with respect to the coherence bandwidth of the channel.

E.1.4.2 Frequency Selective Fading

A mobile radio channel is called frequency selective fading if

$$B_S > B_C \tag{E.12}$$

and

$$T_S < \sigma_\tau \tag{E.13}$$

Frequency selective fading channels are also called as wideband channels, since the bandwidth of the transmitted signal is wider than the coherence bandwidth of the channel [30].

E.2 Rayleigh and Ricean Distributions

E.2.1 Rayleigh Distribution

The Rayleigh distribution is frequently used to describe the envelope of the small-scale fading signal. It is well known that the envelope of the sum of two quadrature Gaussian noise signals obeys a Rayleigh distribution [30]. The probability density function of the Rayleigh distribution is

$$p(r) = \frac{r}{\sigma^2} \exp(-\frac{r^2}{2\sigma^2}) \text{ for } 0 \leq r \leq \infty \tag{E.14}$$

where σ is the rms value of the received voltage signal before envelope detection, and σ^2 is the time-average power of the received signal before envelope detection [30].

E.2.2 Ricean Distribution

The small-scale fading envelope distribution is called Ricean when dominant signal component exists in the received signal. Dominant signal component is seen as a DC

offset at the output of the envelope detector. As the dominant signal component fades, the distribution becomes Rayleigh.

The probability density function of the Ricean Distribution is

$$p(r) = \frac{r}{\sigma^2}\exp(-\frac{r^2+A^2}{2\sigma^2})I_0(\frac{Ar}{\sigma^2}) \text{ for } (A\geq 0, r \geq 0) \tag{E.15}$$

where A denotes the peak amplitude of the dominant signal component, and I_0 is the modified Bessel function of the first kind and zero-order. As $A \to 0$, amplitude of the dominant signal component decreases and the Ricean distribution degrades to a Rayleigh distribution [30].